Structures 63 (2024) 106392

Contents lists available at ScienceDirect

Structures

journal homepage: www.elsevier.com/locate/structures

Elastic lateral-torsional buckling of cellular beams

Luana Vidoti da Silva [a,*], Luís M.R. Mesquita [b,*]

[a] Instituto Politécnico de Bragança, Campus Santa Apolónia, 5300-253 Bragança, Portugal
[b] Grupo de Investigação em Construção Sustentável (GICoS), Instituto Politécnico de Bragança, Campus Santa Apolónia, 5300-253 Bragança, Portugal

ARTICLE INFO

Keywords:
Cellular beams
Lateral torsional buckling
Torsional constant
Numerical simulation
Elastic critical moment

ABSTRACT

Cellular beams are I-shaped steel sections with advantages provided by their circular web openings. This type of beam can have greater spans, be more slender and higher than the solid beams, being more prone to failure by lateral-torsional buckling. Given there is still no specific standard for cellular beams and owing to the importance of safety verification, this paper numerically investigated the lateral-torsional buckling of these beams. Considering the torsional constant as the most important parameter in the design of web-opening beams, this study proposes a new torsional constant and approaches four different calculation methods of weighted average torsional constants. The elastic critical moment of cellular beams was numerically modelled using ANSYS software and compared with analytical results according to European standards, varying the torsional constants. The weighted average torsional constant based on an equivalent area and using the proposed torsional constant was the most efficient, showing the best analytical results when compared with the numerical ones considering the load condition of constant bending moment. Furthermore, from all the geometric parameters evaluated, the height of the cellular beam was what most influenced the elastic critical moment of the cellular beams.

1. Introduction

In building structures, the I-shaped steel sections are a widely used structural element, especially the cellular beams, which provide advantages with the circular openings of the web. Without increasing the height between floors, the cellular beams allow the passage of electrical installations and conduits [1]. Furthermore, structures in some establishments, such as parking garages and schools, usually use this type of beam because it allows longer spans to be supported by fewer columns and footings, creating a floor with flexible space and reducing structural costs [2]. The fabrication process of the steel cellular beams requires two thermal cutting passes of a parent I-section web. Then the two tee sections are repositioned and welded back together [3], creating a cellular beam higher than its parent section.

A common failure mode of stell cellular beams is the lateral-torsional buckling (LTB). This is a type of global buckling failure mechanism that causes both a lateral displacement and a torsional rotation of the cross-section. LTB occurs when the movement of the buckled compressed part of the beam is restrained by the part of the beam in tension [4]. Although the LTB already exists for solid beams, the cellular beams are more prone to failure by LTB because they are slenderer and higher than solid beams [5]. Although web openings must be considered in the design of structures, there is still no specific standard for cellular beams. The proposal to complement Eurocode 3 part 1–13 [6], the Annex N of the ENV 1993 version - 1–1: 1992 [7], the P355 of SCI [3], and the Steel Design Guide 31 of AISIC [2] are some of the only design guides for cellular beams available.

Owing to the importance of safety verification, the lateral buckling modes on castellated, [4,8–12], and cellular beams [1,4,5,13–18] has been constantly investigated by researchers. Sonck [4] examined the global buckling behaviour of cellular and castellated beams, establishing the residual stresses' significant impact on LTB resistance and proposing a new model of residual stress for these beams. De'nan et al. [19] performed a numerical analysis to evaluate the LTB behaviour of different web opening beams, which showed a significant influence of the spacing-to-diameter ratio on it. Komal Rajana et al. [20] studied the influence of the geometric parameters of the cellular beams with elastic and inelastic finite element analysis of them under strong-axis bending and considered the thickness of the web the most critical parameter in both analyses. Kurlapkar et al. [21] analysed the web perforations effect on the buckling behaviour of cellular beams and observed that the spacing-diameter ratio of these beams influenced the failure to be by LTB or LDT.

Depending on the type of cellular beam and its geometrics parameters, the standards and design guides recommend LTB resistance

* Corresponding authors.
E-mail addresses: luanavidotis@gmail.com (L.V. da Silva), lmesquita@ipb.pt (L.M.R. Mesquita).

https://doi.org/10.1016/j.istruc.2024.106392
Received 19 October 2023; Received in revised form 12 February 2024; Accepted 7 April 2024
Available online 13 April 2024

Nomenclature

A_{open}	Equivalent hole opening area
A_{solid}	Solid area between the bottom and top of the hole opening
a_0	Diameter of hole openings
b_f	Flange width
C_1, C_2	Factors depending on the loading and end restraint conditions
d_i	Half web height subtracting the hole opening
E	Modulus of elasticity
F_{cr}	Elastic critical load
$F_{nonlinear}$	Non-linear load
$F_{\exp}$	Experimental load
f_y	Yield strength of steel
G	Shear modulus
H	Final height of the cellular beam
h	Height of solid beam
h_w	Height of web cellular beam
$I_{t,sol}$	Torsional constant for solid beams
$I_{t,2T}$	Torsional constant for 2 t section
$I_{t,hole}$	Torsional constant for cellular beams
$I_{t,avg}$	Weighted average torsional constant
I_w	Warping constant
$I_{z,2T}$	Moment of inertia for 2 T section
k_w, k_z	Effective length factors
L	Beam length
L_f	Distance between the two experimental load points
$M_{b,Rd}$	Resistant moment of LTB
M_{cr}	Elastic critical moment
n	Number of holes
S	Spacing between the holes
t_f	Flange thickness
t_w	Web thickness
U	Displacement along an axis
w	Intermediate web post length
w_{end}	End web post length
z_g	Distance between the load point of application and the shear centre
z_i	Distance along the beam length

approaches considered conservative, uneconomical, or sometimes insecure [13,17,18,22,23]. To better prevent the LTB behaviour of cellular beams, researchers have been bringing different formulas and methods to estimate the LTB of these beams. According to Sweedan [1], the moment-gradient factor for the LTB of cellular beams had a lower value than the values recommended by design codes for the LTB of solid beams, developing, then, a reduction factor for the moment-gradient, which resulted in precise and conservative results. Boissonnade et al. [18] proposed a new group of design rules, which showed to give secure and moderately accurate estimates of the LTB resistance, being similar to EC3 [24] LTB design rules but differing on the use of the buckling curve "c" for all cases and on the use of the weakest cross-section. To improve the design precision about underestimation of LTB resistance in cellular beams of lower slenderness, Panedpojaman et al. [22] proposed a correction factor by a slight adjustment to the General method of EC3, resulting in designs more efficient than the original but still conservative and safe. Phuvoravan and Ponsorn [23] considered it unsafe to use the equation of LTB given in the American standard for evaluating cellular beams with sectional properties at the web-post section, but also conservative when the equation used the sectional properties at the web-opening. Then, they suggested a new factor to reduce the moment capacity from the equation with sectional properties at the web-post section, showing suitable and better results than the other two approaches. Due to the uncertainty about which buckling curve to use in the calculation of the LTB for cellular beams according to the EC3, Ferreira et al. [14] investigated this failure mode and compared it to standards, analytical designs and a possible updating of the EC3. Investigating the LTB behaviour of cellular beams, Bhat and Gupta [25] studied the variation of the moment-gradient factor with different beam lengths according to the Indian Standard and proposed a reduction factor for lower slenderness. Caroline et al. [15] analysed the LTB resistance of cellular steel beams at room and fire temperatures, proposing a new procedure based on European design guidelines, but considering the maximum capacity of the cross-section at the centre of the opening and a modified reduction factor for LTB. Khatri et al. [16] investigated the lateral buckling modes with the effect of three different levels of loading positions on the elastic gradient factor for cellular steel beams. A new equation for the plateau length of the LTB curves based on the mean squared error approach was provided by Oribi et al. [26] after evaluating the LTB resistance of cellular beans at both ambient and high temperatures.

Furthermore, some studies have been investigating the torsional constant influence on the LTB behaviour of web-opening steel beams and the 2 T approach design. Sonck and Belis [5] proposed a weighted average to calculate the torsional constant of cellular beams, considering equivalent rectangular opening lengths, which resulted in better results for larger beam lengths. Carvalho et al. [27] numerically studied the beams with sinusoidal openings and proposed different methods for calculating their elastic critical moment as an alternative to the conventional 2 T approach. Carvalho et al. [28] considered the torsional constant as the most important parameter in the design of web-opening beams and considered the area of the openings and the solid part of the beam rather than an equivalent length as a new method for calculating this constant for beams with sinusoidal openings.

Recent investigations have used intelligence methods to study the LTB resistance of steel beams with web openings. An algorithm based on gene expression programming and nonlinear multiple regression [29], a least square support machine optimized by metaheuristic algorithms [30] and an artificial neural network (ANN) [31–33] are some of them. Furthermore, hybrid cellular steel beams have been investigated in [34–36], as an alternative to address the problem of LTB.

Therefore, considering all these mentioned works and the importance of the torsional constant on the LTB behaviour of cellular beams, this study proposes a new analytic calculation method of the torsional constant, performing numerical linear finite element simulations and analysing the influence of the geometric properties of the cellular beams in the LTB.

2. Desing of cellular beams

2.1. 2 T approach

Depending on the design for a given section, the dimensions of geometric characteristics vary according to their applications and objectives. These dimensions are the diameter (a_0) of the hole openings, the distance (S) between them, the height (h) of the parent I-section of a solid beam that gives rise to the cellular beam, and the final height (H) of the cellular beam. Fig. 1 shows the geometric dimensions of the cellular beam, which are necessary for the cross-section strength calculation.

To calculate the geometric properties of the cellular beams the approach 2 T, based on [11], is adopted. In this approach, which also is repeated in [7], the LTB resistance of a cellular beam can be calculated like the solid beams but using the cross-sectional properties calculated at the centre of the web hole. Then, it is possible to define the moment of

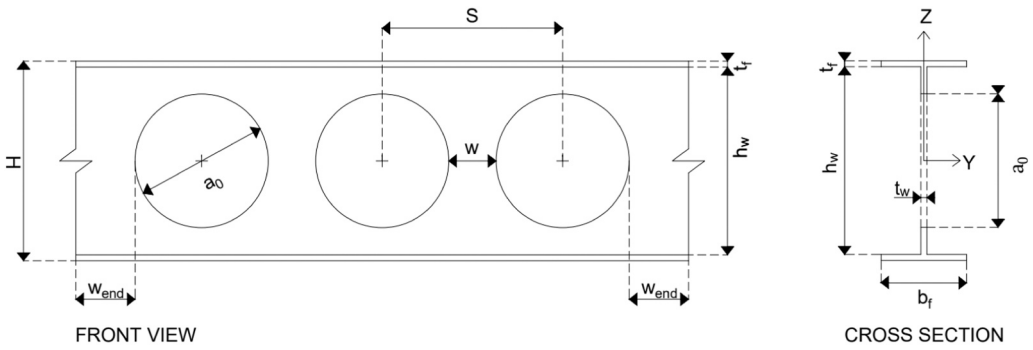

Fig. 1. Geometric dimensions of the cellular beam in front view and cross-section.

inertia $I_{Z,2T}$ given by Eq. (1) and the torsional constant $I_{t,2T}$ given by Eq. (2) of the cellular beams disregarding the radius of agreement between the flange and the web. The web opening almost does not influence on the warping constant [1], so it is considered the same constant used for solid beams given by Eq. (3).

$$I_{Z,2T} = \frac{t_f b_f^3}{6} + \frac{(h_w - a_0)t_w^3}{12} \tag{1}$$

$$I_{t,2T} = \frac{2}{3} b_f t_f^3 + \frac{1}{3}(h_w - a_0)t_w^3 \tag{2}$$

$$I_w = \frac{t_f b_f^3 (h_w + t_f)^2}{24} \tag{3}$$

2.2. Safety verification according to the Eurocode

The safety verification according to the EC3 [24] presented the design of steel structures. To calculate the resistance of LTB $M_{b,Rd}$, the Eurocode 3 considers that the beams are laterally unrestrained and uses the same equation for solid and cellular beams. The difference will be in the geometric parameters of beams, like the constant of torsion. For this calculation, it is necessary to know the reduction factor for LTB, which depends, in addition to other factors, on the critical moment for LTB. The elastic critical moment M_{cr} for LTB is based on cross-sectional properties of the beam and considers the loading and support conditions, and the real moment distribution. According to [37], to bi-symmetric cross-sections, the elastic critical moment is given by Eq. (4).

$$M_{cr} = C_1 \frac{\pi^2 E I_z}{(k_z L)^2} \left\{ \sqrt{\left[\left(\frac{k_z}{k_w} \right)^2 \frac{I_w}{I_z} + \frac{(k_z L)^2 G I_t}{\pi^2 E I_z} + (C_2 Z_g)^2 \right]} - C_2 Z_g \right\} \tag{4}$$

In Eq. (4), G is the shear modulus that depends on the modulus of elasticity E and the Poisson's ratio υ, I_z is the moment of area about the minor axis, I_w is the warping constant, I_t is the torsional constant, L is the length of the beam between points which have lateral restraint, C_1 and C_2 are factors depending on the loading and end restraint conditions, k_z and k_w are effective length factors and z_g is the distance between the point of load application and the shear centre. For constant bending moment $C_1 = 1$, and end-moment loading and transverse loads applied at the shear centre $C_2 Z_g = 0$. According to [37], for mid-span concentrated load $C_1 = 1.35$ and $C_2 = 0.59$. In the case of uniformly distributed loads, their values change to 1.12 and 0.45, respectively. The factor k_z refers to end rotation on plan and k_w refers to end warping. Unless a special provision for warping restraint is made, k_w should be taken as 1, 0. And, for normal conditions of restraint at each end (fork support), $k_z = k_w = 1{,}0$.

2.3. Development of a new torsional constant for cellular beams

For the critical moment, the influence of the openings will be larger due to their effect on the torsional stiffness. As a safe approach, Sonck and Belis [5] numerically confirmed that the existing 2 T design approach is efficient for calculating the critical buckling moment of cellular beams. However, for the larger slenderness values (and relatively longer lengths), an underestimation of the numerical critical moment was visible, caused by the underestimation of the torsional constant. To obtain more accurate results on the critical moment of lateral-torsional buckling, a weighted average of the torsional constant along the length is recommended. This weighted average is based on equivalent opening lengths for rectangular openings, which is determined using a multiplication factor [4,5]. Moreover, Carvalho et al. [28] also proposed a similar approach to ponder the torsional constant for beams with sinusoidal openings, differentiating when considering the equivalent areas instead of lengths.

Due to the importance of the torsional constant on the design of the cellular beams, four different methods of calculating the average torsional constant are approached below. The weighted average is between the torsional constant corresponding to the portion of the beam with holes and the torsional constant corresponding to the portion of the beam without holes, equal to the torsional constant for solid beams $I_{t,sol}$ shown in Eq. (5).

$$I_{t,sol} = \frac{2}{3} b_f t_f^3 + \frac{1}{3} h_w t_w^3 \tag{5}$$

The first two methods use the known constant $I_{t,2T}$ shown in Eq. (2), only differentiating the equivalent rectangular openings for the weighted average. Method 1 uses a unitary factor, which results in equivalent rectangles with sides equal to the diameter of the hole in the cellular beam, see Fig. 2(a). On the other hand, Method 2 uses a factor equal to 0.9, studied and defined by Sonck [4], resulting in equivalent rectangles shown in Fig. 2(b). Eq. (6) and Eq. (7) show, respectively, the calculation of the constant weighted average $I_{t,avg1}$ for the first method, and the constant weighted average $I_{t,avg2}$ for the second method. The number of holes of the cellular beam is defined by n and L is the length of the beam.

$$I_{t,avg1} = \frac{n a_0}{L} I_{t,2T} + \left(1 - \frac{n a_0}{L}\right) I_{t,sol} \tag{6}$$

$$I_{t,avg2} = 0,9 \frac{n a_0}{L} I_{t,2T} + \left(1 - 0,9 \frac{n a_0}{L}\right) I_{t,sol} \tag{7}$$

For the Method 3 and 4 it is proposed a new torsional constant for the web portion with the openings, different from the 2 T approach. It is an exact integration of the torsional constant, subtracting the area of the circular hole. Fig. 3(a) shows the area of integration, where $d_i = \frac{h_w}{2} - z_i$. From the equation of the circumference, it can be defined that $z_i = \sqrt{(a_0/2)^2 - x_i^2}$, and the distance d_i can be written as $d_i = \frac{h_w}{2} -$

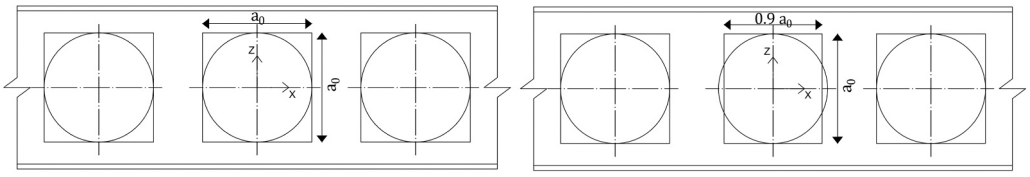

Fig. 2. Equivalent rectangular openings for the calculation of weighted average: (a) $I_{t,avg1}$; (b) $I_{t,avg2}$.

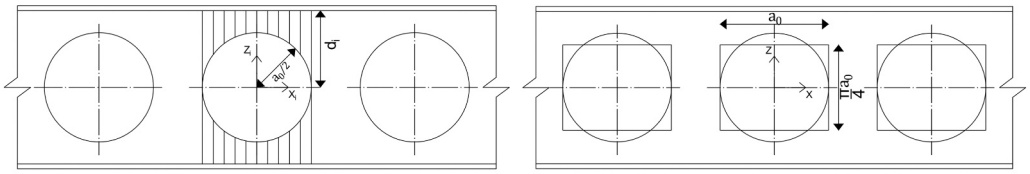

Fig. 3. Method 3, calculation of the new torsional constant $I_{t,hole}$: (a) Area of integration; (b) Equivalent rectangular openings.

$\sqrt{(a_0/2)^2 - x_i^2}$. Therefore, the new torsional constant of the beam portion with the circular hole $I_{t,hole}$ is calculated by Eq. (8). Substituting the value of the distance d_i in Eq. (8), and solving the integral, the final value of the torsional constant $I_{t,hole}$ is determined by Eq. (9). The difference between the constants $I_{t,2T}$ and $I_{t,hole}$ is on the value $\pi/4$ that multiplies a_0 Fig. 3(b) shows equivalent rectangular openings for the calculation of the torsional constant $I_{t,hole}$.

$$I_{t,hole} = \frac{2}{3} b_f t_f^3 + \left[\int_{-a_0/2}^{a_0/2} 2\left(\frac{1}{3} d_i {t_w}^3\right) dx_i \right] \frac{1}{2r} \tag{8}$$

$$I_{t,hole} = \frac{2}{3} b_f t_f^3 + \frac{1}{3}\left(h_w - \frac{\pi a_0}{4}\right) t_w^3 \tag{9}$$

Method 3 uses a unitary factor like the first method for the weighted average calculation $I_{t,avg3}$ shown in Eq. (10) but applies the new proposed constant $I_{t,hole}$ rather than $I_{t,2T}$. Otherwise, Method 4 uses the weighted average proposed in [28] but with the new torsional constant $I_{t,hole}$ in place of $I_{t,2T}$, resulting in the $I_{t,avg4}$ given in Eq. (11). Fig. 4 illustrates the equivalent areas of the Method 4, in which $A_{open} = \pi(a_0/2)^2$.

$$I_{t,avg3} = \frac{n a_0}{L} I_{t,hole} + \left(1 - \frac{n a_0}{L}\right) I_{t,sol} \tag{10}$$

$$I_{t,avg4} = \frac{n A_{open}}{L a_0} I_{t,hole} + \left(1 - \frac{n A_{open}}{L a_0}\right) I_{t,sol} \tag{11}$$

3. Numerical simulations

3.1. Study cases

This parametric study performed analyses of the elastic critical moment on cellular beams based on four types of parent I-sections with the dimensions shown in Table 1. The study explores variations in the final height of the section, diameter, spacing between holes, and beam length across different case studies. Table 2 presents the cases analysed where the reference model (RM) of cellular beams has intermediate values of the geometric parameters. Precisely, RM1 will correspond to IPE 200, RM2 to HE 200 A, RM3 to IPE 360, and RM4 to HE 360 A.

The cellular beams are designed with as many holes as possible for each beam length $(L = (n-1)S + 2w_{end})$, respecting the distance $(S = a_0 + w)$ between the openings. The end web post length (w_{end}) varies for each beam length, ensuring that it is equal to or greater than the intermediate web post (w).

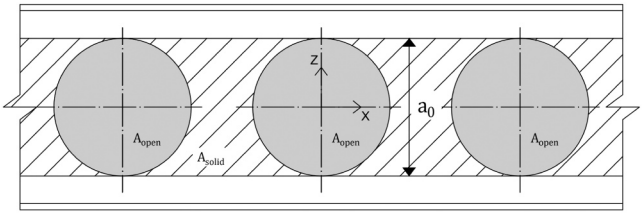

Fig. 4. Method 4, equivalent areas for the calculation of $I_{t,avg4}$.

Table 1
Dimension of the parent I-sections in millimetres.

Profiles	h	b	t_w	t_f
IPE 200	200	100	5.6	8.5
HE 200 A	190	200	6.5	10
IPE 360	360	170	8	12.7
HE 360 A	350	300	10	17.5

3.2. Finite element model

Numerical simulations were performed with the ANSYS Mechanical software, using shell elements in the numerical model, which is suitable for analysing thin to moderately thick shell structures. These simulations were made for an elastic linear analysis, using the Eigenvalue Buckling analysis. The chosen shell element was the SHELL181 with three integration points located through the thickness. Due to the type of analysis performed, the only elastic properties of the material adopted were the modulus of elasticity of 210 GPa and the Poisson's ratio of 0.3. The cross-section is traced by the coordinates of the profile's average surface and the thickness of the surface body is subsequently defined based on

Table 2
Geometric parameters variation of the study cases.

Case	a_0	S	H	$L[m]$
RM	$1.0h$	$1.4a_0$	$1.5h$	1, 1.5, 2, 2.5,..., 9, 9.5, 10
$a_0 = 0.8h$	$0.8h$	$1.4a_0$	$1.5h$	1, 1.5, 2, 2.5,..., 9, 9.5, 10
$a_0 = 1.3h$	$1.3h$	$1.4a_0$	$1.5h$	1, 1.5, 2, 2.5,..., 9, 9.5, 10
$S = 1.1a_0$	$1.0h$	$1.1a_0$	$1.5h$	1, 1.5, 2, 2.5,..., 9, 9.5, 10
$S = 1.7a_0$	$1.0h$	$1.7a_0$	$1.5h$	1, 1.5, 2, 2.5,..., 9, 9.5, 10
$H = 1.3h$	$1.0h$	$1.4a_0$	$1.3h$	1, 1.5, 2, 2.5,..., 9, 9.5, 10
$H = 1.6h$	$1.0h$	$1.4a_0$	$1.6h$	1, 1.5, 2, 2.5,..., 9, 9.5, 10

the geometric dimensions of each profile.

Following the analytical formulae, in which the root radius is disregarded, the numerical model does not consider it explicitly, but its rigidity is partially accounted by the shell elements overlapping areas. Although some studies add additional finite elements to increase the rigidity of this area [38], the root radius has not been considered in most of the recent research related to cellular beams [5,20,26,39].

A structured mesh was defined considering equal element sizes along all straight edges of the beam. The convergence test, illustrated in Fig. 5 (a), was performed on the RM1 with 5 m of length to assess the mesh sensitivity, evaluating element sizes from 55 to 5 mm. The analysis showed an effective convergence from the element size of 10 mm, exhibiting a difference of 1 % compared to the 5 mm mesh and approximately four times fewer elements. Consequently, the numerical model adopted the mesh with element sizes of 10 mm to perform the analyses due to its effective convergence and reduced number of elements. Fig. 5(b) shows the mesh of the web-fragment of the RM1 cellular case.

The boundary conditions representing a simply supported beam with fork supports can be seen in Fig. 6(a). The beams were restrained, on both ends, by the displacement (U_y) in the y-axis direction in the bottom flange, and the displacement (U_x) in the x-axis in the web. Furthermore, the z-displacement (U_z) was constrained at a vertex of only one of the ends. In some cases of short beam lengths, the first buckling mode was not the LTB. To ensure a first buckling mode by LTB, avoiding any local or distortional buckling in the cross-section, the CERIG command was applied in the static structural analysis using the Ansys Parametric Design Language (APDL), which is a structured scripting language used to interact with the Ansys Mechanical solver [40]. This constraint is used to establish rigid-type rotation constraint equations about the z-axis to ensure all nodes of the section have the same rotation degree of freedom [41]. Fig. 6(b) shows the comparison between the cross-section deformation of the RM1 with L= 1.5 m before and after applying the command.

The analyses were performed for different load conditions, applying unit load values to get the elastic critical moment from the eigenvalue buckling mode results. Firstly, a unit moment was applied along the web in the x-axis direction at each end of the beam in opposite directions, as shown in Fig. 7(a), to evaluate the elastic critical moment considering a constant bending moment in all study cases of Table 2. Subsequently, more analyses were carried out only in the reference models considering concentrated and distributed loads to evaluate bending moment gradients and the effects of the load level with respect to the shear centre position. Fig. 7(b) and Fig. 7(c) show the mid-span concentrated loads applied at the top flange (destabilising effect) and bottom flange (stabilising effect), respectively. Since it was not possible to apply the loads directly at the shear centre due to the beams with the circular opening in the middle of the length, in this case, half of the unit load was applied at both flanges [1,16]. Thus, these effects cancel each other out when applied together, creating the neutral effect of the load application at the shear centre illustrated in Fig. 7(d). The uniformly distributed loading was applied only at the top flange, as Fig. 7(e) demonstrates.

4. Finite element model validation

The validation of the numerical model has been carried out in two parts. Firstly, the elastic critical moment of solid beams is numerically determined and compared with the EC3 analytical solution. Secondly, since there are no available experimental results of elastic LTB of cellular beams in the literature, the elastic critical moment and the inelastic behaviour of cellular beams are numerically determined and compared with the experimental tests of [4,5]. Both parts are important for validation. The first analysis verifies the accuracy of modelled boundary conditions and the applied constant moment. The second part is essential to examine the geometry and the adopted mesh of the cellular beams.

4.1. Validation using solid beams

This first part used solid beam numerical cases to validate the numerical model, varying only the length of the beam and comparing the elastic critical moment with the results of the analytical method of EC3, considering only the load condition of the constant bending moment. Each numerical beam model was created with the same mesh, boundary conditions, applied moment and the CERIG command of the parametric study. Furthermore, the numerical model considered the same material elastic properties. The validation used the IPE 200 and HE 200 A solid beam profiles, varying their lengths from 1 to 10 m in increments of 0.5 m.

Table 5 in the Appendix shows the results of the elastic critical moment, and Fig. 8 illustrates the LTB deformed configuration of these solid beam cases with L= 3 m. Fig. 9(a) shows the values of the numerical critical moment as a function of the beam length. The critical moment decreases with the beam length increase. Fig. 9(b) shows the results of the analytical critical moment ($M_{cr,EC3}$) divided by the numerical critical moment ($M_{cr,ANSYS}$). The difference between analytical and numerical methods is less than 1 % in almost all cases, with a slightly larger difference for the shorter lengths of the HE 200 A profile.

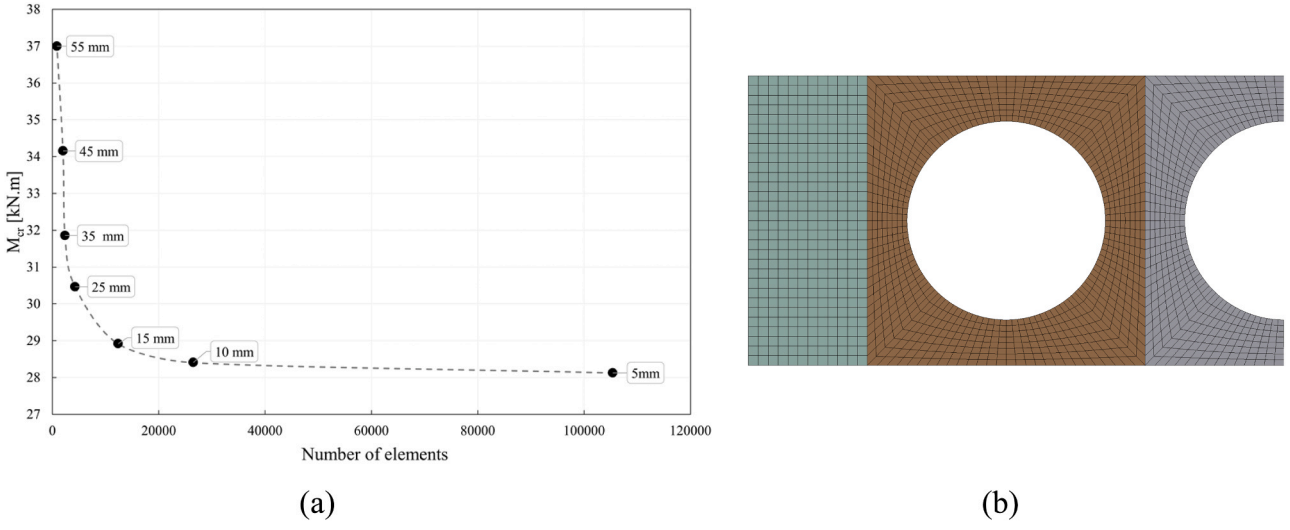

Fig. 5. (a) Mesh sensibility analysis; (b) Web fragment mesh of RM1 cellular case.

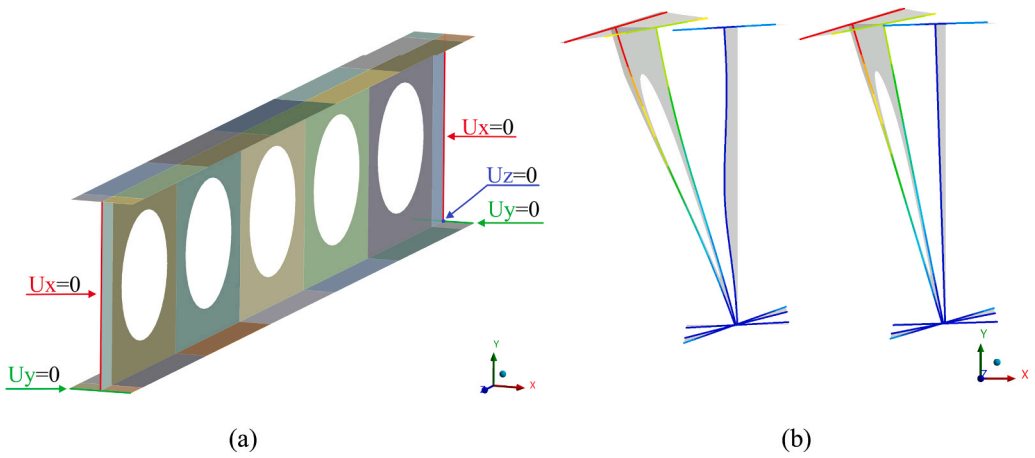

Fig. 6. (a) Numerical model boundary conditions; (b) Comparison between the cross-section deformation without APDL command on left and after applied APDL command on right.

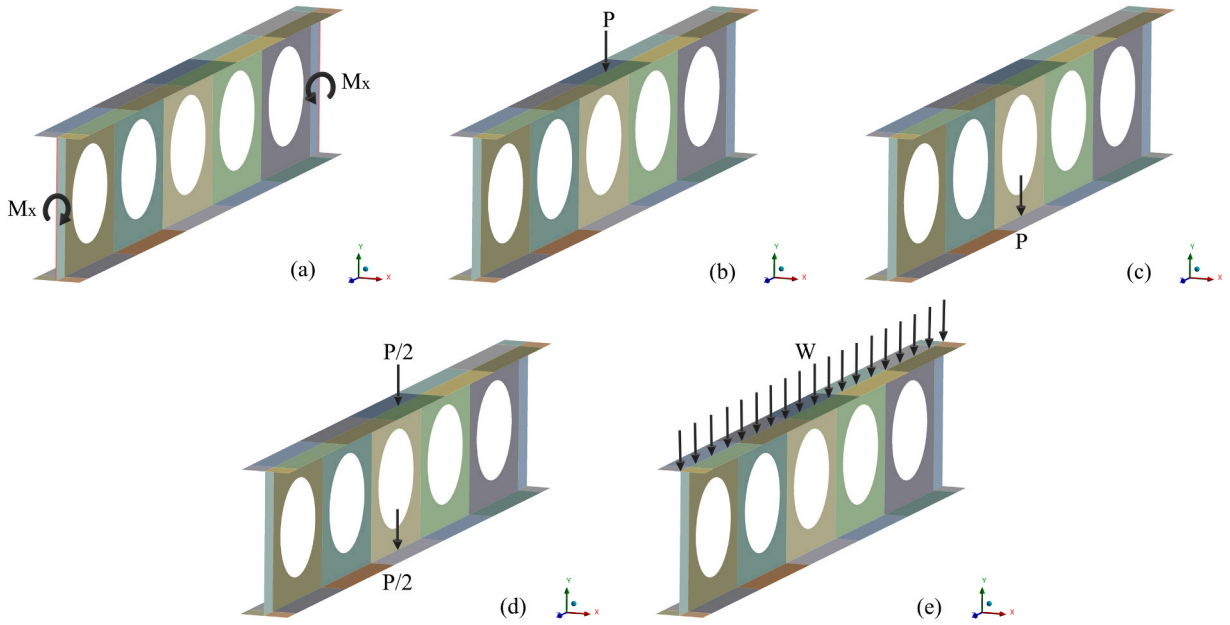

Fig. 7. Loading conditions: (a) Constant bending moment; (b) Concentrated load at top flange; (c) Concentrated load at bottom flange; (d) Concentrated load at shear centre; (e) Distributed load.

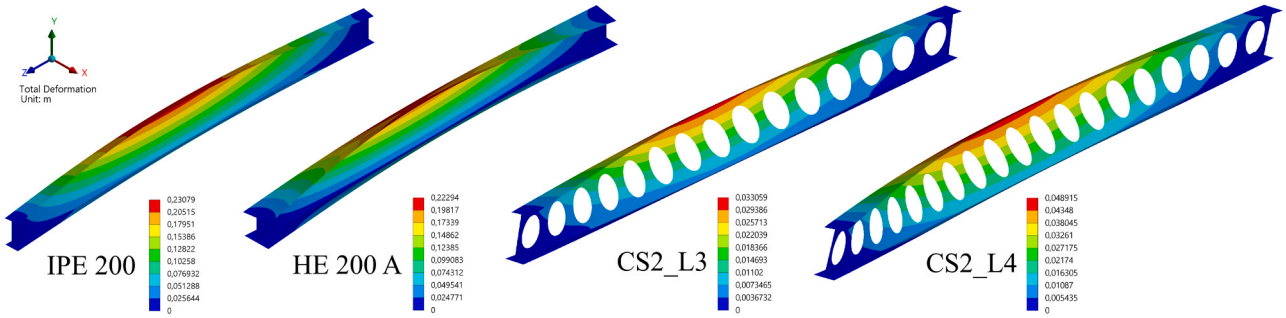

Fig. 8. LTB deformed configuration of the finite element model validation.

For the length L= 1 m of the HE 200 A case, the difference is higher than in all cases because even with the CERIG command applied, the first buckling mode found was not to LTB, and the closest to LTB had any interaction of local or distortional buckling in the cross-section. Therefore, the numerical results show a good agreement with the analytics, validating the boundary conditions and the applied moment of the numerical model.

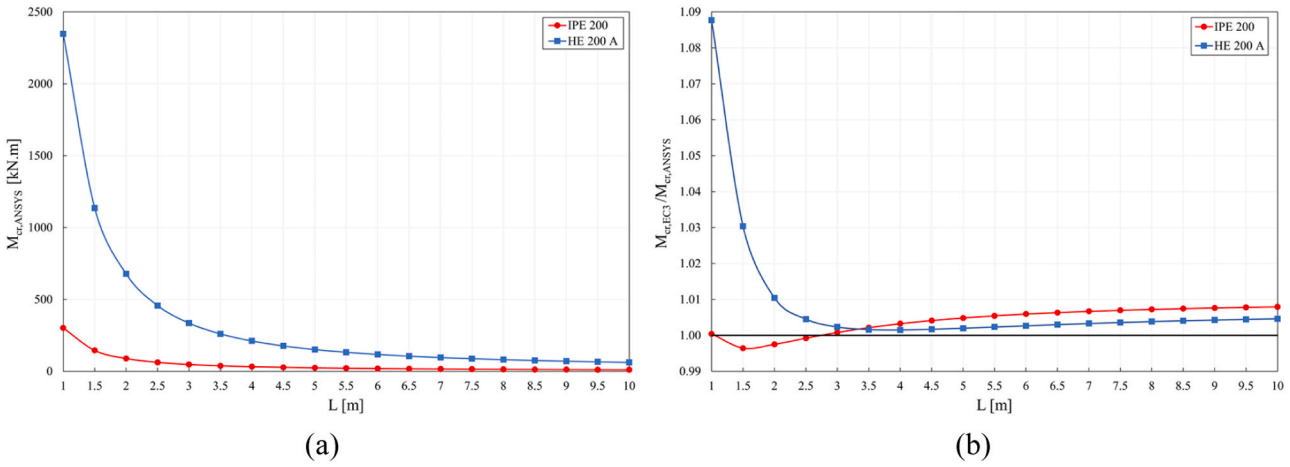

Fig. 9. Validation results of the solid beams cases.

4.2. Validation using cellular beams experimental tests

This second validation part developed buckling and post-buckling analysis to compare the numerical results with the experimental tests. The numerical model was created with the same mesh and boundary conditions (fork support) of the parametric study but using the reworked geometric dimensions from Table 3, which are in accordance with the experimental tests [5]. Furthermore, the beam was now loaded by two-point loads with a distance of L_f between them and the modulus of elasticity was equal to 205 GPa. Fig. 10 illustrates the location of loads and supports for the validation beams.

The buckling linear analysis only considered the elastic material properties, but the post-buckling analysis included material and geometric nonlinearities. The material was modelled by a bilinear stress-strain relationship with a yielding plateau defined by the Eurocode 3 Part 1–5 [42]. Table 3 shows the yield strengths values used, which $f_{y,w}$, $f_{y,tl}$ and $f_{y,bl}$ are the yield strengths of the web and top and bottom flanges, respectively. A global geometric imperfection was applied with the first LTB eigenmode imperfection, obtained from the elastic analyse, using an amplitude of L/1000. Moreover, the numerical non-linear model considered the same initial residual stress used by [26,43,44]. A bitriangular linear distribution model of the residual stress was only applied in the flanges with the residual stress proposed by ECCS [45] for hot-rolled sections, using the command INISTATE. For these cellular beam cases, in which the parent section height-to-width ratio $h/b > 1.2$, the value of compression and tension residual stress is taken to be $0.3f_y$. In the web, the residual stress was null to simplify the numerical model, given that the residual stress in the flanges has more influence in the LTB.

Fig. 8 illustrates the LTB of these cellular beams cases, Table 4 presents the validation results, and Fig. 11 shows the load versus vertical displacement above the loading points of experimental and numerical results. As expected, non-linear analyses resulted in a more realistic behaviour when compared to linear ones, showing the geometric imperfection and residual stress influence. According to Teixeira et al. [46], the selection of the imperfection shape determines the failure mode of the beams, directly affecting the accuracy of the numerical results. They recommend the introduction of the global imperfection in slender beams to achieve greater reliability in LTB.

The elastic critical load ($F_{cr,elastic}$) presents good results when compared with the elastic critical load numerical simulated by Sonck et al. [5] ($F_{cr,[5]}$), with a difference of only 1 % for both cases. Regarding the ratio between the non-linear numerical analysis ($F_{nonlinear}$) and the experimental test ($F_{exp,[5]}$), the load difference is 3 % in the CS2_L4 case and 7 % in the CS2_L3. These numerical results are satisfactory, considering that a simplified initial residual stress and a global imperfection were applied. Therefore, the good agreement between the results validated the numerical model.

5. Results and discussion

Fig. 12 graphically presents the values results of the numerical critical moment in the function of the beam length, comparing all load conditions for each reference model. The critical moment decreases significantly with increasing beam length. Comparing the lowest profiles (RM1 and RM2) with the highest (RM3 and RM4), there is a large increase in the critical moment as the height of the cross-section increases. The influence of the flange slenderness can also be noted when comparing profiles with similar heights. For example, the moment capacity of RM2, which has more slender flanges, is much greater than that of RM1, which has less slender flanges. The same can be seen when comparing RM3 and RM4. Furthermore, critical moment values considering the concentrated load applied at the shear centre and bottom flange are considerably higher than those derived from applying a constant bending moment.

In sequence, it is compared the results obtained by the elastic numerical finite element method with the analytical method of simplified calculation according to Eurocode 3, to analyse the new torsional constant $I_{t,hole}$ and the four different weighted average methods for the torsional constant. A small verification study showed that the other properties of the cross-section have little influence on the elastic critical moment, not justifying the weighting. The difference between using the $I_{Z,2T}$ and the weighted I_Z is only approximately 0.05 % in the elastic critical moment calculation of the RM cellular beams considering constant bending moment. Therefore, the weighted average is applied only to the torsional constant, and the other cross-sectional properties are calculated as shown in Section 2.1.

Table 3
Materials and geometric details of the experiments executed by [5].

Specimen	H[mm]	b_f [mm]	t_w [mm]	t_f [mm]	a_0 [mm]	S [mm]	n	L [mm]	L_f [mm]	$f_{y,tf}$ [MPa]	$f_{y,bf}$ [MPa]	$f_{y,w}$ [MPa]
CS2_L3	220	83.1	5.5	7.3	142.8	67.2	15	3150	210	342	341	329
CS2_L4	220	83.1	5.5	7.3	142.8	67.2	19	3990	1890	348	351	339

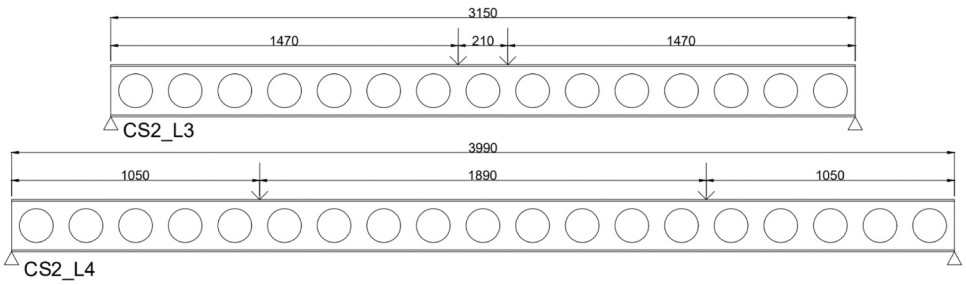

Fig. 10. Location of loads and supports for the validation beams (dimensions in mm).

Table 4
Validation results and comparison between them.

Specimen	$F_{exp,}$ [5] [kN]	$F_{cr,}$[5] [kN]	$F_{cr,}$ elastic [kN]	$F_{nonlinear}$ [kN]	$F_{cr,}$ elastic/ $F_{cr,}$[5]	$F_{nonlinear}$/ $F_{exp,}$[5]
CS2_L3	22.34	27.8	27.63	24.01	0.99	1.07
CS2_L4	23.62	25.9	25.76	24.22	0.99	1.03

5.1. Constant bending moment

Firstly, the basic case of the elastic critical moment, that considers the constant bending moment, is analysed comparing the difference between the analytical and numerical methods. Table 6–9 in the appendix show the results of the elastic critical moment for LTB, considering the constant bending moment for the RM1, RM2, RM3 and RM4, respectively. Fig. 13 illustrates examples of the LTB deformed configuration of these cases with L= 3 m.

To better understand these differences, Fig. 14 shows the analytical critical moment ($M_{cr,EC3}$) divided by the numerical one ($M_{cr,ANSYS}$) in the function of the beam length, varying the torsional constant. Except in the RM4 case, the results of the analytical method using the constant $I_{t,avg4}$ are the closest to the numerical results, continuing to be safe but less conservative. For the longer beam lengths in the RM4 case, constant $I_{t,avg4}$ showed slightly unsafe results, while constants $I_{t,avg2}$ and $I_{t,avg3}$ gave safer results.

The analytical results are higher than the numerical ones for the first short beam lengths of some profiles due to the same behaviour already observed in the validation model using the solid beams, in which the numerical model had the interaction of local or distortional buckling and global LTB. However, it has already been confirmed in some studies of non-linear numerical analysis [5,47] that the effects of plasticity reduce this unsafety observed for shorter beam lengths. As the failure of the geometry is governed by plastic yielding rather than elastic buckling, this difference between the numerical and analytical moment has less influence, and it is not necessary to consider the web distortion in the design rule.

Moreover, a comparison was made only between the analytical results. Fig. 15 presents the percentage relative differences between the critical moments using the four different weighted average methods of torsional constant with the constant $I_{t,2T}$, where some plateaus can be seen, except for the RM3 case. This plateau occurs because the number of cellular beam holes does not increase constantly in these other cases. All weighted average methods have higher values to the critical moment than the constant $I_{t,2T}$, with the weighted averages $I_{t,avg3}$ and $I_{t,avg4}$ being the furthest. This behaviour was expected because Methods 3 and 4 use the torsional constant $I_{t,hole}$, which is the closer constant of the real cellular beam model, increasing the rigidity of the beam and, consequently, the elastic critical moment. The difference between the torsional constants is more considerable in the RM1 and RM3, probably due to the geometry of the profiles, since the RM2 and RM4 have a slenderness flange that is bigger than the other two.

5.1.1. Influence of the geometric parameters

Table 10–13 in the appendix show the results of the elastic critical moment for LTB, considering the constant bending moment for the cases of IPE 200, HE 200 A, IPE 360 and HE 360 A, respectively. The influence of the geometric parameters of the other cases in Table 2 is numerically compared with RM cases, considering three beam lengths. Generally, the variation of the diameter and spacing at L= 3 m had less influence than for longer lengths. However, this behaviour changes when analysing the variation of final height, which has less influence at L= 9 m than at the shorter lengths.

Fig. 16(a) and Fig. 16(b) compared the numerical results between the

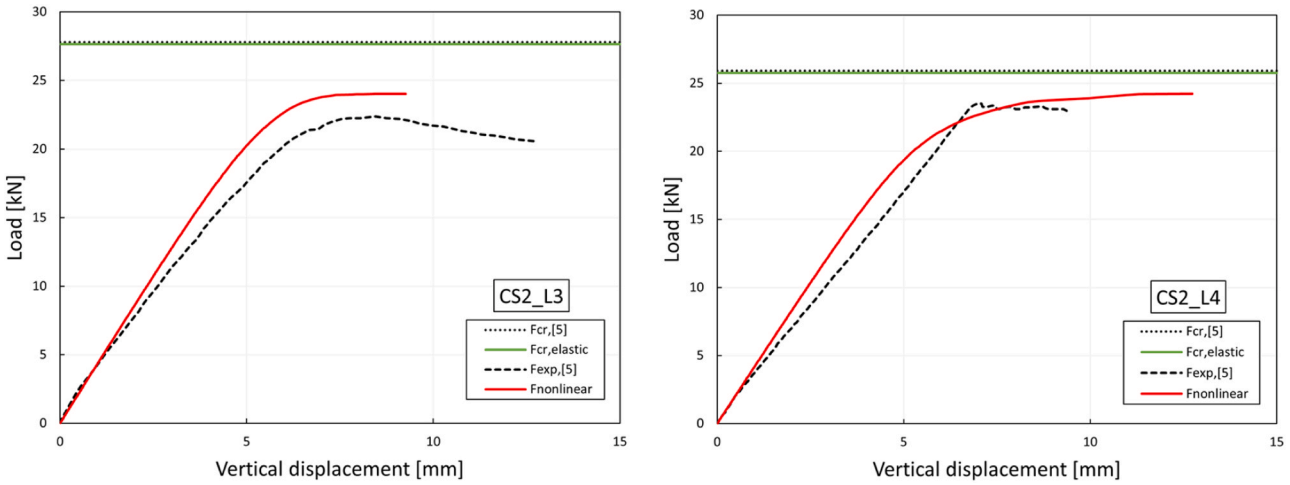

Fig. 11. Load versus vertical displacement of experimental and numerical results.

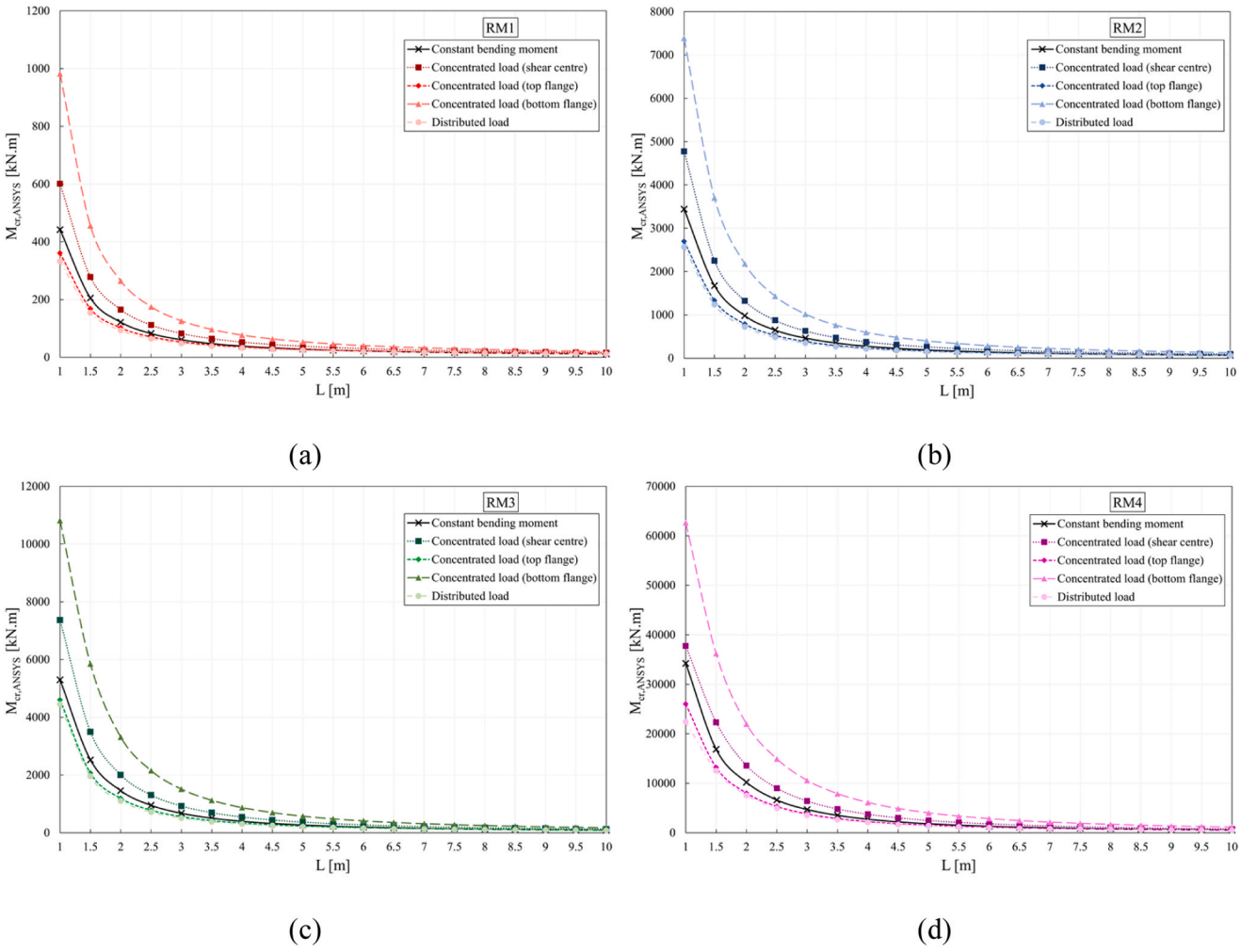

Fig. 12. Numerical elastic critical moment for all conditions loads: (a) RM1; (b) RM2; (c) RM3; (d) RM4.

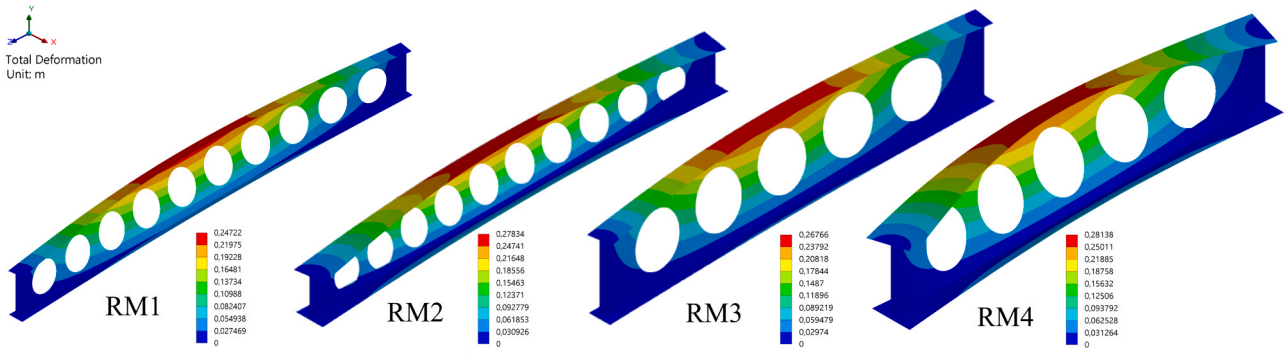

Fig. 13. LTB deformed configuration of the reference cases.

cases varying a_0 with the reference models. The larger the diameter of the hole, the lower the elastic critical moment. Despite the tendency on the behaviour of the moment variation, the influence of the diameter is not linear. The diameter of the hole did not vary the moment by more than 2 % for these lengths of beam profiles analysed. The numerical results of the cases, considering the variations of S, were compared with the reference models in Fig. 16(c) and Fig. 16(d). Unlike the hole diameter, the greater the spacing, the greater the critical moment. The difference in critical moment varying the spacing between the openings is also not very high, not exceeding 2.5 % in all the profiles analysed.

Fig. 16(e) and Fig. 16(f) show the influence of the H variation on the critical moment. As with the spacing between the holes, the greater the height of the beam, the greater the elastic critical moment for LTB. The height is the geometric parameter that most influenced, reaching a difference of approximately 12 %, at H = 1.3h in L= 3 m, in the reference cases of the IPE 360 A, HE 200 A and HE 360 A profiles. For the IPE 200 reference model, this difference reached around 10 %. In the results of the IPE 200 case, considering the a_0 and S variation, the difference between the critical moment is greater than in the HE A cases. When the variation of H is considered, this difference is smaller for IPE 200 than in

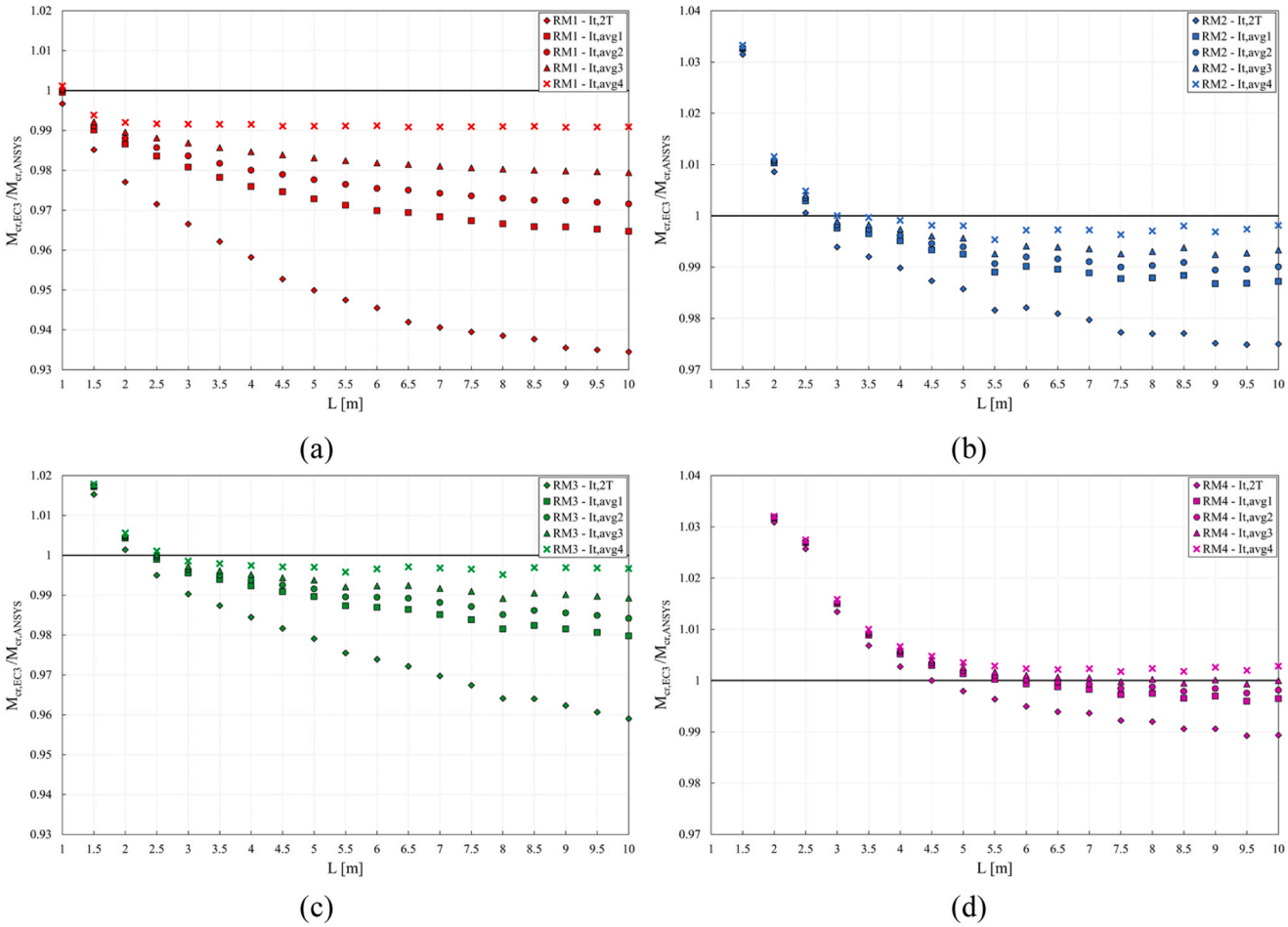

Fig. 14. $M_{cr,EC3}/M_{cr,ANSYS}$: (a) RM1; (b) RM2; (c) RM3; (d) RM4.

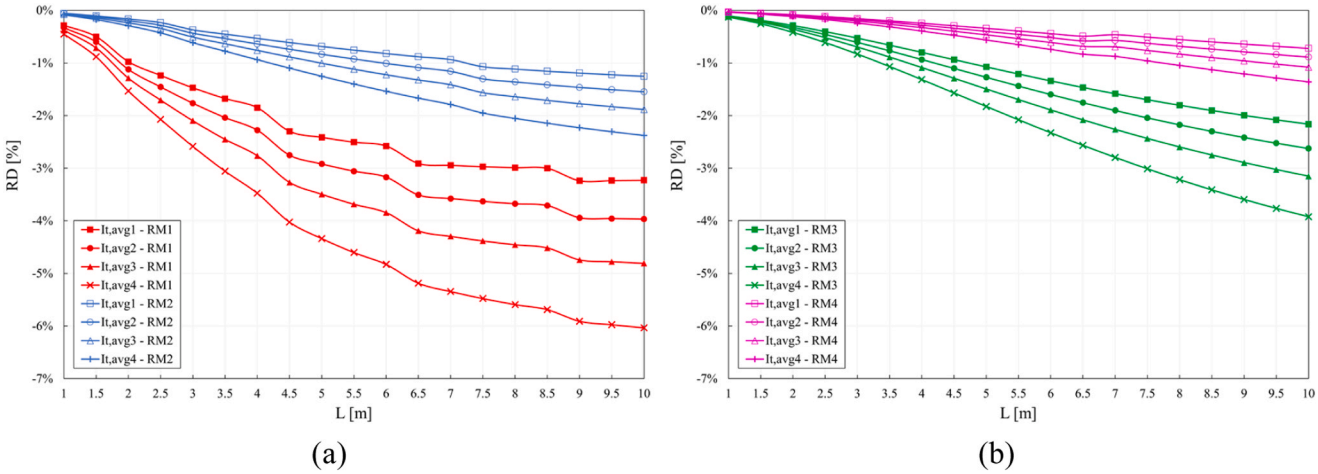

Fig. 15. Percentage relative difference, $RD = \frac{M_{cr}(I_{t,2T}) - M_{cr}(I_{t,avg_i})}{M_{cr}(I_{t,2T})}$ [%].

the other cases.

5.2. Concentrated and distributed loads

Table 14–17 in the appendix show the results of the critical moment considering the concentrated and distributed loads for the RM1, RM2, RM3 and RM4, respectively. Since the constant $I_{t,avg4}$ provides the best analytical results in the mostly cases of constant bending moment, the comparison between the analytical critical moment using this constant ($M_{cr,I_{t,avg4}}$) and the numerical one is presented in Fig. 17, considering all conditions loads.

Except in the cases considering concentrated load at the bottom flange, the results of the analytical method using the constant $I_{t,avg4}$ are mostly safe. The values for concentrated load at the shear centre and distributed load are conservatives with a difference of less than 2 %. The cases considering the concentrated load at the bottom flange presented

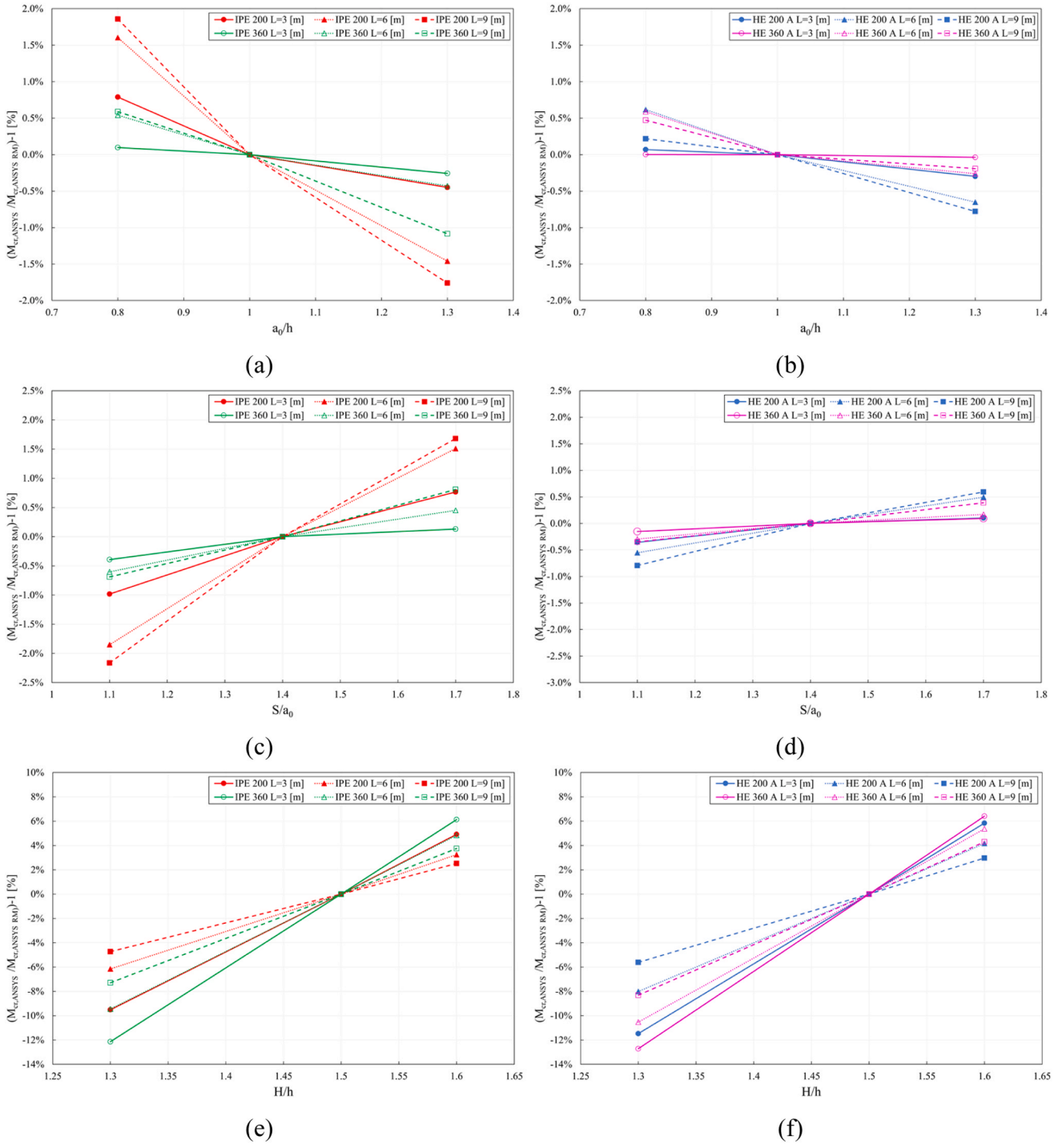

Fig. 16. Numerical comparison between the RM cases and the cases varying the geometrics parameters.

non-conservative results, especially for the RM4, where the difference is up to 5%. However, the values for concentrated load at the top flange, which is the worst load application scenario, the difference is only around 3 % in favour of safety. The destabilising and stabilising effects of the load application point are more evident for shorter beam lengths, where the critical moment is greater than for longer lengths, and these effects have a greater influence.

In Eq. (4) it is recognized that the torsional constant does not directly influence the C_2 coefficient, which is associated with load application effects. Therefore, the proposed method utilizing the constant $I_{t,avg4}$ also demonstrates efficiency in determining the critical moment for LTB in these scenarios involving load conditions that cause gradient moments.

6. Conclusions

A new torsional constant was proposed, and different weight average calculation methods of the torsional constant for cellular beams were approached in this study. To analyse the influence of these torsional constants in the elastic critical moment for LTB, a parametric study was developed, carrying out numerical analysis with finite element models in the ANSYS Mechanical software. The numerical model was first validated with the elastic critical moment analyses of solid beam cases,

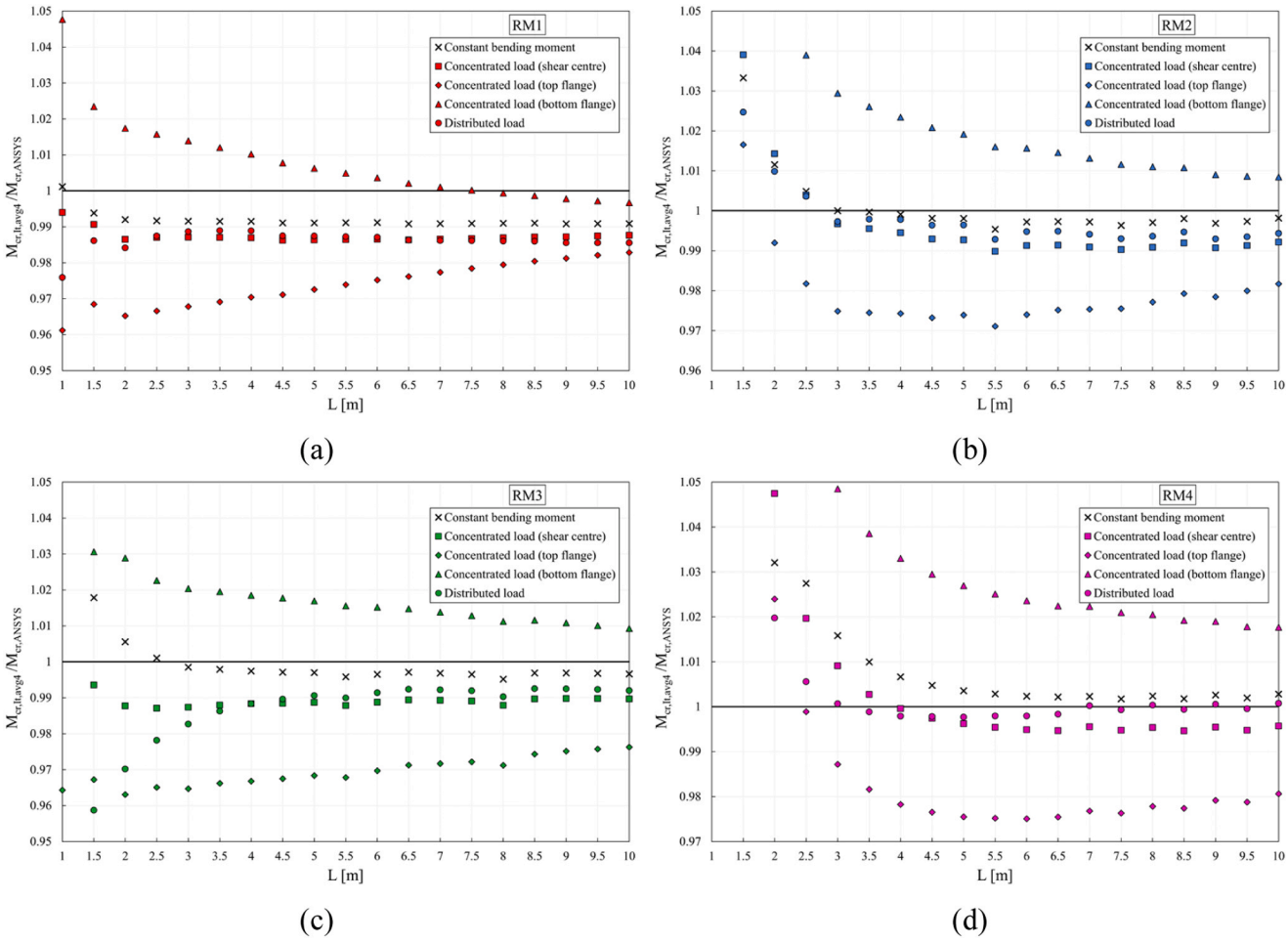

Fig. 17. $M_{cr,It,avg4}/M_{cr,ANSYS}$ (a) RM1; (b) RM2; (c) RM3; (d) RM4.

showing accordance with the EC3 analytics results, and, posteriorly, was compared and validated with a numerical and experimental study of cellular beams, which resulted in a satisfactory agreement.

Through the analysis of the parametric study, the numerical results were compared with the ones obtained using the simplified analytical method of EC3, and the influence of the geometrics parameters in the critical moment was evaluated. In summary, the results indicate the following conclusions:

- In general, the critical moment has a significant decrease with the length increase of the beam. Profiles with a lower cross-section and flange slenderness also have the elastic critical moment reduced;
- The values of critical moment considering the concentrated load applied at the shear centre and bottom flange are considerably higher than those derived from applying a constant bending moment;
- The weighted average torsional constant approached by Method 4 presented the best analytical results compared to the numerical ones, considering the load condition of the constant bending moment. They are in favour of safety and are less conservative than the other methods, except for the cases considering the higher parent profile (HE 360 A), which showed slightly unsafe results;
- Evaluating the geometric parameters variation for the condition of constant bending moment, the larger the hole diameter, the higher the critical moment. When increasing the spacing between the openings and the height of the beam, the critical moment also increases. The height of the beam is the geometric parameter that most influences the critical moment when comparing different beam lengths for the same type of profile;
- The proposed method utilizing the constant $I_{t,avg4}$ is efficient in determining the critical moment for LTB, considering the load conditions that involve gradient moments. The comparison values between the analytical and numerical critical moments presented a small percentage difference and are mostly safe, except for the concentrated load at the bottom flange, which presented slightly non-conservative results.

Declaration of Competing Interest

The authors declare that they have no known competing financial interests or personal relationships that could have appeared to influence the work reported in this paper.

Appendix

Table 5. Elastic critical moments for the validation cases of the solid beam profiles IPE 200 and HE 200 A.

L [m]	$M_{cr,EC3}$ [kN.m]		$M_{cr,ANSYS}$ [kN.m]	
	IPE 200	HE 200 A	IPE 200	HE 200 A
1	302.43	2553.45	302.29	2347.51
1.5	145.25	1170.47	145.77	1135.98
2	89.54	685.45	89.76	678.35
2.5	63.17	459.99	63.22	457.92
3	48.39	336.64	48.35	335.85
3.5	39.11	261.48	39.03	261.06
4	32.81	212.01	32.70	211.69
4.5	28.27	177.50	28.15	177.20
5	24.85	152.31	24.73	152.00
5.5	22.19	133.24	22.07	132.92
6	20.05	118.36	19.93	118.04
6.5	18.30	106.46	18.18	106.14
7	16.84	96.76	16.72	96.44
7.5	15.60	88.69	15.49	88.37
8	14.53	81.88	14.42	81.57
8.5	13.60	76.07	13.50	75.76
9	12.79	71.04	12.69	70.74
9.5	12.07	66.66	11.98	66.36
10	11.43	62.79	11.34	62.51

Table 6. Elastic critical moments for the RM1 considering the constant bending moment.

L [m]	RM1					
	$M_{cr,EC3}$ [kN.m]					$M_{cr,ANSYS}$ [kN.m]
	$I_{t,2T}$	$I_{t,avg1}$	$I_{t,avg2}$	$I_{t,avg3}$	$I_{t,avg4}$	
1	440.65	441.91	442.10	442.31	442.63	442.11
1.5	202.58	203.59	203.80	204.03	204.37	205.64
2	119.05	120.22	120.39	120.59	120.88	121.85
2.5	80.20	81.19	81.37	81.57	81.86	82.55
3	58.91	59.78	59.95	60.15	60.44	60.95
3.5	45.92	46.69	46.86	47.05	47.33	47.73
4	37.36	38.05	38.21	38.39	38.65	38.99
4.5	31.37	32.09	32.23	32.39	32.63	32.92
5	26.98	27.64	27.77	27.93	28.15	28.41
5.5	23.66	24.25	24.38	24.53	24.75	24.97
6	21.06	21.60	21.72	21.87	22.07	22.27
6.5	18.97	19.53	19.64	19.77	19.96	20.14
7	17.27	17.78	17.89	18.01	18.19	18.36
7.5	15.85	16.32	16.42	16.54	16.72	16.87
8	14.65	15.09	15.19	15.30	15.47	15.61
8.5	13.62	14.03	14.13	14.24	14.40	14.53
9	12.73	13.15	13.24	13.34	13.49	13.61
9.5	11.96	12.34	12.43	12.53	12.67	12.79
10	11.27	11.64	11.72	11.81	11.95	12.06

Table 7. Elastic critical moments for the RM2 considering the constant bending moment.

L [m]	RM2					
	$M_{cr,EC3}$ [kN.m]					$M_{cr,ANSYS}$ [kN.m]
	$I_{t,2T}$	$I_{t,avg1}$	$I_{t,avg2}$	$I_{t,avg3}$	$I_{t,avg4}$	
1	3841.00	3843.17	3843.46	3843.79	3844.28	3439.62
1.5	1729.60	1731.43	1731.74	1732.10	1732.63	1676.81
2	990.33	991.98	992.30	992.67	993.22	981.88
2.5	647.88	649.39	649.72	650.09	650.64	647.50
3	461.57	463.28	463.58	463.92	464.41	464.41
3.5	348.97	350.55	350.84	351.18	351.67	351.78
4	275.62	277.09	277.39	277.72	278.21	278.45
4.5	225.10	226.48	226.76	227.09	227.57	227.99
5	188.74	190.04	190.32	190.64	191.11	191.47
5.5	161.64	162.86	163.13	163.44	163.90	164.67
6	140.84	142.00	142.26	142.56	143.01	143.41
6.5	124.49	125.58	125.84	126.13	126.56	126.91
7	111.36	112.40	112.65	112.94	113.35	113.67
7.5	100.64	101.71	101.95	102.21	102.60	102.98

(continued on next page)

(*continued*)

L [m]	RM2					
	$M_{cr,EC3}$ [kN.m]					$M_{cr,ANSYS}$ [kN.m]
	$I_{t,2T}$	$I_{t,avg1}$	$I_{t,avg2}$	$I_{t,avg3}$	$I_{t,avg4}$	
8	91.74	92.76	92.99	93.24	93.62	93.90
8.5	84.25	85.22	85.44	85.69	86.06	86.23
9	77.88	78.80	79.02	79.26	79.61	79.86
9.5	72.39	73.28	73.48	73.72	74.06	74.26
10	67.63	68.48	68.68	68.90	69.24	69.36

Table 8. Elastic critical moments for the RM3 considering the constant bending moment.

L [m]	RM3					
	$M_{cr,EC3}$ [kN.m]					$M_{cr,ANSYS}$ [kN.m]
	$I_{t,2T}$	$I_{t,avg1}$	$I_{t,avg2}$	$I_{t,avg3}$	$I_{t,avg4}$	
1	5723.87	5729.85	5730.18	5730.57	5731.13	5294.88
1.5	2565.70	2570.52	2570.96	2571.47	2572.22	2527.13
2	1460.17	1464.38	1464.88	1465.44	1466.27	1458.12
2.5	948.29	952.11	952.63	953.22	954.09	953.08
3	670.04	673.58	674.11	674.72	675.61	676.60
3.5	502.09	505.41	505.94	506.55	507.44	508.50
4	392.90	396.03	396.56	397.17	398.07	399.09
4.5	317.87	320.84	321.37	321.97	322.86	323.80
5	264.03	266.87	267.39	267.99	268.86	269.67
5.5	224.05	226.76	227.27	227.86	228.71	229.67
6	193.50	196.09	196.59	197.17	198.00	198.69
6.5	169.59	172.08	172.57	173.12	173.94	174.45
7	150.50	152.88	153.36	153.90	154.70	155.19
7.5	134.98	137.27	137.73	138.26	139.04	139.53
8	122.17	124.37	124.83	125.34	126.10	126.72
8.5	111.46	113.58	114.02	114.53	115.26	115.62
9	102.40	104.44	104.87	105.36	106.08	106.41
9.5	94.64	96.61	97.03	97.51	98.20	98.52
10	87.95	89.85	90.26	90.72	91.40	91.71

Table 9. Elastic critical moments for the RM4 considering the constant bending moment.

L [m]	RM4					
	$M_{cr,EC3}$ [kN.m]					$M_{cr,ANSYS}$ [kN.m]
	$I_{t,2T}$	$I_{t,avg1}$	$I_{t,avg2}$	$I_{t,avg3}$	$I_{t,avg4}$	
1	41597.43	41609.45	41610.10	41610.84	41611.93	34203.34
1.5	18585.97	18595.78	18596.63	18597.62	18599.06	16880.81
2	10531.47	10540.14	10541.10	10542.20	10543.81	10216.06
2.5	6802.87	6810.82	6811.83	6812.99	6814.70	6632.56
3	4776.91	4784.36	4785.40	4786.60	4788.35	4713.72
3.5	3554.78	3561.84	3562.90	3564.11	3565.89	3530.61
4	2761.03	2767.77	2768.83	2770.05	2771.84	2753.49
4.5	2216.31	2222.78	2223.84	2225.06	2226.85	2216.27
5	1826.16	1832.39	1833.44	1834.66	1836.44	1829.96
5.5	1537.00	1543.01	1544.06	1545.26	1547.02	1542.62
6	1316.60	1322.40	1323.44	1324.62	1326.37	1323.27
6.5	1144.62	1150.23	1151.25	1152.42	1154.14	1151.63
7	1007.73	1012.39	1013.47	1014.72	1016.54	1014.19
7.5	896.88	901.45	902.51	903.72	905.50	903.92
8	805.78	810.24	811.28	812.47	814.21	812.29
8.5	729.92	734.28	735.29	736.45	738.16	736.83
9	666.00	670.26	671.26	672.39	674.05	672.31
9.5	611.59	615.76	616.72	617.83	619.46	618.23
10	564.84	568.91	569.85	570.93	572.52	570.92

Table 10. Elastic critical moments for the IPE 200 cases, varying the geometric parameters and considering the constant bending moment.

L [m]	IPE 200											
	M_{cr} [kN.m]				M_{cr} [kN.m]				M_{cr} [kN.m]			
	Analytical EC3		ANSYS		Analytical EC3		ANSYS		Analytical EC3		ANSYS	
	$I_{t,avg4}$				$I_{t,avg4}$				$I_{t,avg4}$			
	$a_0 = 0.8h$	$a_0 = 1.3h$	$a_0 = 0.8h$	$a_0 = 1.3h$	$S = 1.1a_0$	$S = 1.7a_0$	$S = 1.1a_0$	$S = 1.7a_0$	$H = 1.3h$	$H = 1.6h$	$H = 1.3h$	$H = 1.6h$
1	442.89	442.35	441.37	442.00	442.24	443.02	441.06	442.96	385.29	471.45	385.15	470.70
1.5	204.70	204.29	206.14	205.64	204.12	204.86	205.12	206.38	179.59	216.88	180.55	218.32
2	121.06	120.41	122.22	121.42	120.52	121.06	121.22	122.27	107.42	127.71	108.15	128.82
2.5	82.09	81.55	83.27	82.17	81.46	82.13	81.81	83.03	73.55	86.10	74.00	86.93
3	60.63	60.23	61.43	60.68	60.12	60.65	60.35	61.41	54.87	63.29	55.15	63.94
3.5	47.54	47.04	48.46	47.22	47.07	47.58	47.25	48.21	43.38	49.36	43.55	49.90
4	38.88	38.44	39.47	38.82	38.38	38.86	38.44	39.43	35.72	40.17	35.83	40.63
4.5	32.80	32.31	33.30	32.49	32.34	32.80	32.38	33.30	30.37	33.79	30.49	34.20
5	28.30	27.90	28.79	28.05	27.91	28.30	27.95	28.76	26.37	29.08	26.44	29.44
5.5	24.90	24.54	25.37	24.69	24.54	24.91	24.56	25.32	23.29	25.50	23.35	25.82
6	22.24	21.85	22.63	21.95	21.86	22.22	21.86	22.61	20.87	22.70	20.90	23.00
6.5	20.09	19.74	20.45	19.85	19.74	20.08	19.73	20.44	18.94	20.48	18.98	20.76
7	18.33	18.01	18.82	18.10	18.00	18.30	18.00	18.64	17.32	18.64	17.35	18.90
7.5	16.84	16.52	17.19	16.69	16.52	16.84	16.49	17.15	15.96	17.11	15.98	17.34
8	15.59	15.30	16.04	15.39	15.29	15.58	15.27	15.88	14.80	15.81	14.81	16.03
8.5	14.52	14.22	14.80	14.28	14.24	14.51	14.22	14.79	13.80	14.70	13.81	14.91
9	13.59	13.31	13.86	13.37	13.33	13.57	13.32	13.84	12.95	13.76	12.97	13.96
9.5	12.77	12.52	13.04	12.65	12.51	12.77	12.48	13.01	12.19	12.92	12.20	13.10
10	12.05	11.79	12.32	11.84	11.81	12.04	11.78	12.28	11.51	12.18	11.52	12.35

Table 11. Elastic critical moments for the HE 200 A cases, varying the geometric parameters and considering the constant bending moment.

L [m]	HE 200 A											
	M_{cr} [kN.m]				M_{cr} [kN.m]				M_{cr} [kN.m]			
	Analytical EC3		ANSYS		Analytical EC3		ANSYS		Analytical EC3		ANSYS	
	$I_{t,avg4}$				$I_{t,avg4}$				$I_{t,avg4}$			
	$a_0 = 0.8h$	$a_0 = 1.3h$	$a_0 = 0.8h$	$a_0 = 1.3h$	$S = 1.1a_0$	$S = 1.7a_0$	$S = 1.1a_0$	$S = 1.7a_0$	$H = 1.3h$	$H = 1.6h$	$H = 1.3h$	$H = 1.6h$
1	3844.66	3843.86	3473.84	3364.91	3843.69	3844.87	3516.28	3515.46	3324.90	4104.54	3003.72	3815.45
1.5	1733.14	1731.86	1678.06	1677.45	1731.86	1733.02	1683.19	1678.16	1504.85	1847.06	1457.55	1786.93
2	993.61	992.76	981.66	981.66	992.65	993.79	980.95	983.05	867.36	1056.65	857.73	1044.50
2.5	651.10	650.36	649.75	647.58	650.20	651.09	646.77	649.42	571.81	690.52	569.02	687.29
3	464.73	463.75	464.73	463.03	463.69	464.78	462.75	464.88	411.02	491.53	411.11	491.51
3.5	351.95	351.17	352.39	351.13	351.07	351.97	350.87	352.62	313.49	371.15	313.48	371.37
4	278.53	277.61	279.18	277.79	277.57	278.59	277.17	279.30	249.80	292.76	249.85	293.14
4.5	227.93	227.09	228.65	227.33	227.02	227.90	227.13	228.78	205.77	238.78	205.98	239.33
5	191.42	190.56	192.25	190.74	190.63	191.39	190.76	192.14	173.97	199.95	174.13	200.46
5.5	164.24	163.45	165.86	163.55	163.40	164.23	163.43	164.85	150.15	171.02	150.76	171.91
6	143.36	142.50	144.29	142.47	142.56	143.30	142.62	144.12	131.79	148.84	131.93	149.38
6.5	126.88	126.14	127.41	126.18	126.10	126.89	126.15	127.58	117.27	131.41	117.42	131.86
7	113.68	112.99	114.22	113.02	112.94	113.65	112.96	114.36	105.56	117.42	105.57	117.92
7.5	102.88	102.15	103.46	102.23	102.18	102.86	102.18	103.55	95.99	106.06	96.22	106.55
8	93.87	93.23	94.44	93.29	93.19	93.86	93.17	94.40	87.95	96.59	88.04	96.97
8.5	86.32	85.64	86.75	85.62	85.67	86.31	86.04	86.80	81.16	88.63	81.18	88.91
9	79.85	79.25	80.04	79.24	79.26	79.85	79.23	80.34	75.34	81.86	75.38	82.23
9.5	74.31	73.68	74.63	73.63	73.70	74.28	73.69	74.81	70.30	76.04	70.33	76.40
10	69.49	68.89	69.69	68.92	68.91	69.47	68.84	69.87	65.91	70.99	65.90	71.22

Table 12. Elastic critical moments for the IPE 360 cases, varying the geometric parameters and considering the constant bending moment.

L [m]	IPE 360											
	M_{cr} [kN.m]				M_{cr} [kN.m]				M_{cr} [kN.m]			
	Analytical EC3		ANSYS		Analytical EC3		ANSYS		Analytical EC3		ANSYS	
	$I_{t,avg4}$				$I_{t,avg4}$				$I_{t,avg4}$			
	$a_0 = 0.8h$	$a_0 = 1.3h$	$a_0 = 0.8h$	$a_0 = 1.3h$	$S = 1.1a_0$	$S = 1.7a_0$	$S = 1.1a_0$	$S = 1.7a_0$	$H = 1.3h$	$H = 1.6h$	$H = 1.3h$	$H = 1.6h$
1	5731.40	5728.43	5271.77	5334.71	5729.06	5731.13	4616.44	5625.80	4959.39	6117.58	4616.44	5625.80
1.5	2572.71	2569.76	2525.39	2526.10	2570.85	2572.22	2196.79	2692.03	2231.88	2742.89	2196.79	2692.03
2	1466.93	1465.56	1458.68	1458.82	1465.26	1467.28	1270.52	1552.22	1276.82	1561.46	1270.52	1552.22
2.5	954.87	953.03	954.09	952.41	952.50	954.89	833.59	1013.17	834.38	1014.38	833.59	1013.17
3	676.05	674.31	677.26	674.87	674.30	676.26	594.50	718.04	593.69	716.97	594.50	718.04
3.5	508.00	505.99	509.38	506.61	506.35	507.99	448.89	538.63	448.22	537.42	448.89	538.63
4	398.70	397.30	400.20	398.27	396.66	398.53	354.14	421.90	353.51	420.68	354.14	421.90
4.5	323.55	321.92	324.95	322.65	321.64	323.66	288.78	341.58	288.28	340.45	288.78	341.58
5	269.36	267.79	270.82	268.33	267.79	269.56	241.71	283.88	241.36	282.89	241.71	283.88

(continued on next page)

(*continued*)

L [m]	IPE 360											
	M_{cr} [kN.m]				M_{cr} [kN.m]				M_{cr} [kN.m]			
	Analytical EC3		ANSYS		Analytical EC3		ANSYS		Analytical EC3		ANSYS	
	$I_{t,avg4}$				$I_{t,avg4}$				$I_{t,avg4}$			
	$a_0 = 0.8h$	$a_0 = 1.3h$	$a_0 = 0.8h$	$a_0 = 1.3h$	$S = 1.1a_0$	$S = 1.7a_0$	$S = 1.1a_0$	$S = 1.7a_0$	$H = 1.3h$	$H = 1.6h$	$H = 1.3h$	$H = 1.6h$
5.5	229.27	227.56	230.79	227.95	227.77	229.34	206.98	241.26	206.41	240.12	206.98	241.26
6	198.60	197.26	199.76	197.84	196.89	198.56	179.91	208.30	179.60	207.43	179.91	208.30
6.5	174.56	173.10	175.60	173.46	172.94	174.44	158.66	182.54	158.54	181.85	158.66	182.54
7	155.20	153.79	156.35	153.97	153.80	155.15	141.77	162.09	141.65	161.42	141.77	162.09
7.5	139.56	138.08	140.59	138.17	138.23	139.65	127.96	145.45	127.86	144.80	127.96	145.45
8	126.64	125.41	127.78	125.57	125.18	126.65	116.71	131.87	116.43	131.09	116.71	131.87
8.5	115.82	114.52	116.57	114.72	114.42	115.77	106.82	120.14	106.82	119.62	106.82	120.14
9	106.54	105.29	107.03	105.25	105.30	106.54	98.65	110.40	98.65	109.92	98.65	110.40
9.5	98.68	97.38	99.01	97.30	97.50	98.63	91.59	102.08	91.62	101.61	91.59	102.08
10	91.88	90.77	92.11	90.88	90.61	91.92	85.53	94.90	85.53	94.44	85.53	94.90

Table 13. Elastic critical moments for the HE 360 A cases, varying the geometric parameters and considering the constant bending moment.

L [m]	HE 360 A											
	M_{cr} [kN.m]				M_{cr} [kN.m]				M_{cr} [kN.m]			
	Analytical EC3		ANSYS		Analytical EC3		ANSYS		Analytical EC3		ANSYS	
	$I_{t,avg4}$				$I_{t,avg4}$				$I_{t,avg4}$			
	$a_0 = 0.8h$	$a_0 = 1.3h$	$a_0 = 0.8h$	$a_0 = 1.3h$	$S = 1.1a_0$	$S = 1.7a_0$	$S = 1.1a_0$	$S = 1.7a_0$	$H = 1.3h$	$H = 1.6h$	$H = 1.3h$	$H = 1.6h$
1	41612.35	41606.86	32245.05	33145.19	41607.94	41611.93	38833.61	34045.24	35923.81	44458.67	30268.69	30445.62
1.5	18599.96	18594.38	17020.07	17594.10	18596.42	18599.06	17424.67	16943.31	16085.13	19858.56	14719.32	17957.57
2	10545.07	10542.48	10249.44	10197.39	10539.87	10545.78	10222.00	10189.12	9140.54	11247.87	8923.83	10866.06
2.5	6815.20	6812.65	6627.24	6632.80	6811.58	6816.26	6619.09	6634.94	5925.21	7261.78	5770.64	7065.44
3	4789.20	4785.82	4713.84	4711.95	4785.78	4789.64	4706.51	4718.10	4177.67	5095.93	4114.41	5015.45
3.5	3566.98	3563.03	3531.83	3527.18	3562.63	3566.98	3524.97	3532.06	3123.05	3789.45	3092.62	3751.56
4	2773.11	2770.33	2755.76	2752.64	2769.03	2772.78	2747.89	2755.44	2437.67	2940.97	2421.41	2921.42
4.5	2227.72	2224.97	2217.92	2214.43	2224.39	2227.67	2212.05	2217.93	1966.93	2358.73	1957.03	2347.66
5	1837.46	1834.29	1832.16	1827.34	1834.26	1837.88	1830.24	1832.58	1629.41	1941.77	1623.04	1935.18
5.5	1548.16	1544.66	1544.77	1539.71	1544.44	1548.31	1538.84	1546.98	1378.92	1632.78	1374.08	1628.45
6	1327.23	1323.85	1331.07	1319.82	1324.05	1327.52	1319.36	1325.53	1187.69	1397.31	1183.98	1394.40
6.5	1155.11	1152.40	1153.78	1149.67	1152.05	1155.19	1152.13	1153.80	1038.19	1213.62	1034.89	1211.36
7	1018.06	1015.10	1017.64	1012.60	1014.63	1017.97	1011.76	1016.86	918.42	1067.00	915.03	1065.00
7.5	907.05	903.89	906.35	901.45	903.76	906.81	900.87	908.24	821.68	948.72	819.00	947.54
8	815.52	812.46	820.27	809.93	812.62	815.41	813.44	815.25	741.97	851.55	739.01	849.99
8.5	739.49	736.29	739.12	733.68	736.69	739.62	734.24	738.97	675.41	770.66	673.03	769.74
9	675.40	672.67	675.48	671.02	672.36	675.40	669.97	674.93	619.16	702.55	616.42	701.17
9.5	620.82	617.96	620.53	616.18	617.89	620.71	618.80	620.41	571.14	644.59	568.90	643.75
10	573.70	570.94	578.20	568.93	571.07	573.68	568.69	575.21	529.74	594.82	527.19	593.57

Table 14. Elastic critical moments for RM1 considering the concentrated and distributed loads.

L [m]	RM1							
	M_{cr} [kN.m]							
	Concentrated load						Distributed load	
	Shear centre		Top flange		Bottom flange			
	Analytical EC3 $I_{t,avg4}$	ANSYS	Analytical EC3 $I_{t,avg4}$	ANSYS	Analytical EC3 $I_{t,avg4}$	ANSYS	Analytical EC3 $I_{t,avg4}$	ANSYS
1	597.55	601.17	346.92	360.94	1029.24	982.37	324.84	332.86
1.5	275.90	278.50	163.19	168.51	466.44	455.76	152.24	154.38
2	163.19	165.42	98.84	102.40	269.42	264.80	91.78	93.26
2.5	110.51	111.96	68.67	71.05	177.84	175.08	63.43	64.24
3	81.59	82.66	52.06	53.79	127.87	126.11	47.83	48.38
3.5	63.89	64.73	41.85	43.18	97.55	96.39	38.24	38.66
4	52.18	52.87	35.05	36.12	77.69	76.91	31.85	32.21
4.5	44.05	44.66	30.31	31.22	64.01	63.51	27.41	27.76
5	38.01	38.53	26.74	27.49	54.03	53.69	24.06	24.37
5.5	33.41	33.87	23.98	24.63	46.54	46.31	21.48	21.76
6	29.80	30.21	21.79	22.35	40.75	40.60	19.44	19.70
6.5	26.94	27.32	20.05	20.54	36.20	36.13	17.82	18.07
7	24.56	24.89	18.56	18.99	32.49	32.45	16.44	16.67
7.5	22.57	22.87	17.30	17.69	29.43	29.43	15.27	15.49
8	20.88	21.16	16.22	16.56	26.88	26.90	14.28	14.48
8.5	19.44	19.69	15.28	15.59	24.72	24.76	13.41	13.60
9	18.21	18.44	14.48	14.75	22.90	22.95	12.67	12.86
9.5	17.11	17.32	13.74	13.99	21.30	21.36	12.00	12.18
10	16.13	16.34	13.08	13.31	19.90	19.97	11.40	11.57

Table 15. Elastic critical moments for RM2 considering the concentrated and distributed loads.

L [m]	RM2							
	M_{cr} [kN.m]							
	Concentrated load						Distributed load	
	Shear centre		Top flange		Bottom flange			
	Analytical EC3 $I_{t,avg4}$	ANSYS	Analytical EC3 $I_{t,avg4}$	ANSYS	Analytical EC3 $I_{t,avg4}$	ANSYS	Analytical EC3 $I_{t,avg4}$	ANSYS
1	5189.77	4773.94	2981.07	2696.44	9034.93	7389.95	30190.62	22423.75
1.5	2339.06	2251.17	1353.04	1331.00	4043.64	3703.50	13525.30	12509.31
2	1340.85	1321.99	782.92	789.25	2296.38	2179.30	7691.76	7542.74
2.5	878.37	874.90	518.73	528.38	1487.35	1431.51	4991.07	4963.46
3	626.96	629.01	375.14	384.81	1047.80	1017.84	3523.45	3521.11
3.5	474.76	476.91	288.12	295.66	782.31	762.46	2637.97	2641.00
4	375.58	377.65	231.35	237.46	609.72	595.77	2062.71	2067.01
4.5	307.22	309.41	192.18	197.47	491.13	481.13	1667.79	1671.43
5	257.99	259.89	163.91	168.30	406.07	398.43	1384.79	1388.00
5.5	221.27	223.53	142.78	147.03	342.90	337.49	1174.90	1177.33
6	193.06	194.76	126.49	129.87	294.66	290.10	1014.79	1016.88
6.5	170.86	172.34	113.63	116.52	256.92	253.23	889.73	891.21
7	153.03	154.43	103.25	105.86	226.80	223.85	789.57	789.37
7.5	138.51	139.87	94.78	97.17	202.41	200.09	708.80	709.26
8	126.39	127.55	87.65	89.70	182.24	180.26	642.30	642.07
8.5	116.18	117.12	81.60	83.33	165.40	163.63	586.82	587.17
9	107.48	108.48	76.42	78.10	151.16	149.80	539.98	539.69
9.5	99.98	100.86	71.92	73.39	139.00	137.81	500.02	500.24
10	93.47	94.20	67.98	69.24	128.52	127.44	465.58	465.24

Table 16. Elastic critical moments for RM3 considering the concentrated and distributed loads.

L [m]	RM3							
	M_{cr} [kN.m]							
	Concentrated load						Distributed load	
	Shear centre		Top flange		Bottom flange			
	Analytical EC3 $I_{t,avg4}$	ANSYS	Analytical EC3 $I_{t,avg4}$	ANSYS	Analytical EC3 $I_{t,avg4}$	ANSYS	Analytical EC3 $I_{t,avg4}$	ANSYS
1	7737.03	7363.58	4436.10	4600.33	13494.20	10814.75	4163.73	4451.66
1.5	3472.50	3495.03	2000.82	2068.65	6026.64	5847.73	1876.19	1956.96
2	1979.47	2004.03	1148.15	1192.18	3412.68	3316.86	1075.25	1108.29
2.5	1288.02	1304.88	753.23	780.49	2202.53	2153.72	704.27	719.99
3	912.07	923.73	538.46	558.16	1544.92	1514.09	502.53	511.37
3.5	685.05	693.42	408.73	423.04	1148.17	1126.20	380.66	385.95
4	537.39	543.75	324.32	335.46	890.45	874.27	301.35	304.91
4.5	435.86	440.96	266.24	275.18	713.55	701.12	246.79	249.37
5	362.96	367.10	224.49	231.84	586.82	577.05	207.57	209.53
5.5	308.76	312.55	193.43	199.86	492.87	485.32	178.38	180.19
6	267.30	270.33	169.62	174.93	421.24	414.93	156.01	157.37
6.5	234.82	237.33	150.93	155.40	365.33	360.01	138.45	139.52
7	208.85	211.11	135.96	139.92	320.81	316.45	124.38	125.36
7.5	187.71	189.78	123.73	127.27	284.76	281.16	112.90	113.82
8	170.24	172.32	113.59	116.96	255.13	252.30	103.38	104.40
8.5	155.60	157.22	105.07	107.84	230.44	227.80	95.39	96.10
9	143.20	144.68	97.82	100.31	209.64	207.40	88.58	89.25
9.5	132.58	133.95	91.57	93.85	191.94	190.03	82.73	83.37
10	123.39	124.67	86.15	88.24	176.73	175.10	77.64	78.27

Table 17. Elastic critical moments for RM4 considering the concentrated and distributed loads.

L [m]	RM4							
	M_{cr} [kN.m]							
	Concentrated load						Distributed load	
	Shear centre		Top flange		Bottom flange			
	Analytical EC3 $I_{t,avg4}$	ANSYS	Analytical EC3 $I_{t,avg4}$	ANSYS	Analytical EC3 $I_{t,avg4}$	ANSYS	Analytical EC3 $I_{t,avg4}$	ANSYS
1	56176.10	37752.50	32155.09	26004.76	98141.69	62650.00	30190.62	22423.75
1.5	25108.74	22335.29	14413.32	13213.71	43740.70	36196.23	13525.30	12509.31
2	14234.14	13589.05	8202.99	8010.99	24699.64	21986.74	7691.76	7542.74
2.5	9199.84	9022.33	5327.87	5333.85	15885.73	14943.75	4991.07	4963.46
3	6464.27	6405.99	3765.49	3814.39	11097.33	10583.95	3523.45	3521.11
3.5	4813.95	4800.91	2822.84	2875.71	8209.50	7904.77	2637.97	2641.00
4	3741.99	3743.59	2210.47	2259.57	6334.63	6132.08	2062.71	2067.01
4.5	3006.24	3013.99	1790.08	1833.08	5048.67	4904.11	1667.79	1671.43
5	2479.19	2488.57	1488.84	1526.23	4128.30	4019.91	1384.79	1388.00
5.5	2088.48	2098.07	1265.44	1297.59	3446.81	3362.44	1174.90	1177.33
6	1790.59	1799.76	1095.03	1123.02	2927.99	2860.52	1014.79	1016.88
6.5	1558.09	1566.41	961.93	986.12	2523.74	2468.41	889.73	891.21
7	1372.33	1378.46	855.28	875.58	2201.95	2153.83	789.57	789.37
7.5	1222.43	1228.88	769.32	787.97	1942.41	1902.57	708.80	709.26
8	1099.19	1104.29	698.55	714.38	1729.59	1694.89	642.30	642.07
8.5	996.51	1001.88	639.51	654.28	1552.82	1523.53	586.82	587.17
9	909.97	914.12	589.65	602.20	1404.30	1378.15	539.98	539.69
9.5	836.27	840.67	547.11	558.96	1278.26	1255.90	500.02	500.24
10	772.90	776.24	510.44	520.53	1170.31	1149.95	465.58	465.24

References

[1] Sweedan AMI. Elastic lateral stability of I-shaped cellular steel beams. J Constr Steel Res 2011;vol. 67(2):151–63. https://doi.org/10.1016/J.JCSR.2010.08.009.

[2] Fares SS, Coulson J, Dinehart DW. Steel design guide 31: castellated and cellular beam design. Am Inst Steel Constr 2016.

[3] Lawson RM, Hicks SJ. Design of composite beams with large web openings: in accordance with Eurocodes and the UK National Annexes, P355 ed. SCI 2011.

[4] Sonck D. Global Buckling of Castellated and Cellular Steel Beams and Columns. Ghent University; 2014.

[5] Sonck D, Belis J. Lateral-torsional buckling resistance of cellular beams. J Constr Steel Res 2015;vol. 105:119–28. https://doi.org/10.1016/j.jcsr.2014.11.003.

[6] CEN, 'Draft - EN 1993–1-13, Eurocode 3 - Part 1.13: Steel Beams with Large Web Openings'. European Committee for Standardization, Brussels, Belgium, 2017.

[7] CEN, 'ENV 1993–1-1:1992/A2, Annex N, Eurocode 3: Design of steel structures - Part 1–1: General rules and rules for buildings'. European Committee for Standardization, Brussels, 1992.

[8] Ellobody E. Interaction of buckling modes in castellated steel beams. J Constr Steel Res 2011;vol. 67(5):814–25. https://doi.org/10.1016/J.JCSR.2010.12.012.

[9] Muhammed Jasir T, Raj MP. Numerical investigation on behaviour of castellated steel beam in lateral distortional buckling. Mater Today Proc 2022;vol. 65: 3874–80. https://doi.org/10.1016/J.MATPR.2022.07.172.

[10] Kerdal D, Nethercott DA. Failure modes for castellated beams. J Constr Steel Res 1984;vol. 4:295–315.

[11] Kerdal D. Lateral-Torsional Buckling Strength of Castellated Beams. University of Sheffield; 1982.

[12] Mohebkhah A. The moment-gradient factor in lateral–torsional buckling on inelastic castellated beams. J Constr Steel Res 2004;vol. 60(10):1481–94. https://doi.org/10.1016/J.JCSR.2004.02.002.

[13] Panedpojaman P. Investigation on lateral torsional buckling resistance of EC3 for cellular beam. Int J Adv Mech Civ Eng 2015;no. 2:30.

[14] Ferreira FPV, Rossi A, Martins CH. Lateral-torsional buckling of cellular beams according to the possible updating of EC3. J Constr Steel Res 2019;vol. 153: 222–42. https://doi.org/10.1016/J.JCSR.2018.10.011.

[15] Correa de Faria C, Carvalho H, Hallal Fakury R, Figueiredo Grilo L. Lateral-torsional buckling resistance of cellular steel beams at room temperature and fire situation. Eng Struct 2021;vol. 237:112046. https://doi.org/10.1016/J.ENGSTRUCT.2021.112046.

[16] Khatri AP, Katikala SR, Kotapati VK. Effect of load height on elastic buckling behavior of I-shaped cellular beams. Structures 2021;vol. 33:1923–35. https://doi.org/10.1016/J.ISTRUC.2021.05.047.

[17] Ertenli MF, Erdal E, Buyukkaragoz A, Kalkan I, Aksoylu C, Özkılıç YO. Lateral torsional buckling of doubly-symmetric steel cellular I-Beams. Steel Compos Struct 2023;vol. 46(5):709–18. https://doi.org/10.12989/scs.2023.46.5.709.

[18] Boissonnade N, Nseir J, Lo M, Somja H. Design of cellular beams against lateral torsional buckling. Struct Build 2014;vol. 167(7):436–44. https://doi.org/10.1680/stbu.12.00049.

[19] De'nan F, Nazri FM, Hashim NS. Finite element analysis on lateral torsional buckling behaviour of I-beam with web opening. Eng Herit J 2017;vol. 1(2):19–22. https://doi.org/10.26480/gwk.02.2017.19.22.

[20] Rajana K, Tsavdaridis KD, Koltsakis E. , 'Elastic and inelastic buckling of steel cellular beams under strong-axis bending'. Thin-Walled Struct 2020;vol. 156: 106955. https://doi.org/10.1016/J.TWS.2020.106955.

[21] Kurlapkar RR, Patil AP, Kumbhar PD. Analyzing the influence of perforations on the structural behavior of mild steel cellular beams. Asian J Civ Eng 2023;vol. 1: 1–10. https://doi.org/10.1007/S42107-023-00849-1.

[22] Panedpojaman P, Sae-Long W, Chub-Uppakarn T. Cellular beam design for resistance to inelastic lateral–torsional buckling. Thin-Walled Struct 2016;vol. 99: 182–94. https://doi.org/10.1016/J.TWS.2015.08.026.

[23] Phuvoravan K, Ponsorn P. Nonlinear finite element analysis to evaluate lateral torsional buckling moment of elliptical cellular steel beams. Eng J 2017;vol. 21(1): 93–108. https://doi.org/10.4186/ej.2017.21.1.93.

[24] CEN, 'EN 1993–1-1, Eurocode 3 - Design of steel structures - Part 1–1: General rules and rules for buildings'. European Committee for Standardization, Brussels, Belgium, 2005.

[25] Bhat RA, Gupta LM. Moment-gradient factor for perforated cellular steel beams under lateral torsional buckling. Arab J Sci Eng 2020;vol. 45:8727–43. https://doi.org/10.1007/s13369-020-04836-5.

[26] Oribi SB, Kada A, Lamri B, Mesquita L. Behaviour of cellular steel beams at ambient and high-temperature conditions. J Constr Steel Res 2023;vol. 207:107969. https://doi.org/10.1016/J.JCSR.2023.107969.

[27] Carvalho AS, Rossi A, Martins CH. Assessment of lateral–torsional buckling in steel I-beams with sinusoidal web openings. Thin-Walled Struct 2022;vol. 175:109242. https://doi.org/10.1016/J.TWS.2022.109242.

[28] Carvalho AS, Oliveira VM, Rossi A, Martins CH. Elastic lateral-torsional buckling behavior of steel I-beams with sinusoidal web openings. Structures 2023;vol. 47: 23–36. https://doi.org/10.1016/J.ISTRUC.2022.11.027.

[29] Moghbeli A, Sharifi Y. New predictive equations for lateral-distortional buckling capacity assessment of cellular steel beams. Structures 2021;vol. 29:911–23. https://doi.org/10.1016/J.ISTRUC.2020.12.004.

[30] Ben Seghier MEA, Carvalho H, Faria CC, Correia JAFO, Fakury RH. Numerical analysis and prediction of lateral-torsional buckling resistance of cellular steel beams using FEM and least square support vector machine optimized by metaheuristic algorithms. Alex Eng J 2023;vol. 67:489–502. https://doi.org/10.1016/J.AEJ.2022.12.062.

[31] Ferreira FPV, Shamass R, Limbachiya V, Tsavdaridis KD, Martins CH. Lateral–torsional buckling resistance prediction model for steel cellular beams generated by Artificial Neural Networks (ANN). Thin-Walled Struct 2022;vol. 170: 108592. https://doi.org/10.1016/J.TWS.2021.108592.

[32] Carvalho AS, Hosseinpour M, Rossi A, Martins CH, Sharifi Y. New formulas for predicting the lateral–torsional buckling strength of steel I-beams with sinusoidal web openings. Thin-Walled Struct 2022;vol. 181:110067. https://doi.org/10.1016/J.TWS.2022.110067.

[33] Sharifi Y, Moghbeli A, Hosseinpour M, Sharifi H. Study of neural network models for the ultimate capacities of cellular steel beams. Iran J Sci Technol, Trans Civ Eng 2020;vol. 44:579–89. https://doi.org/10.1007/s40996-019-00281-z.

[34] Desai RB, Khatri AP. Behavioural comparison between hybrid cellular steel beams and homogeneous cellular steel beams for different spans. Asian J Civ Eng 2023; vol. 24(8):3767–80. https://doi.org/10.1007/S42107-023-00751-W.
[35] Desai RB, Khatri AP. Performance of laterally unrestrained hybrid cellular steel beams. Asian J Civ Eng 2023;vol. 24(8):2755–65. https://doi.org/10.1007/S42107-023-00672-8.
[36] Sehwail MM, Celikag M. Load carrying capacity of hot-rolled hybrid cellular steel beams: experimental investigations. Arab J Sci Eng 2022;vol. 47(10):12633–48. https://doi.org/10.1007/S13369-021-06508-4.
[37] Boissonnade N, Greiner R, Jaspart JP, Lindner J. Rules for member stability in EN 1993-1-1. Background Documentation and Design Guidelines, vol. 119. Brussels, Belgium: ECCS; 2006.
[38] Boissonnade N, Nseir J, Somja H. Experimental and numerical investigations towards the lateral torsional buckling of cellular steel beams. Thin-Walled Struct 2024;vol. 195:111388. https://doi.org/10.1016/J.TWS.2023.111388.
[39] Valeš J, Stan TC. FEM modelling of lateral-torsional buckling using shell and solid elements. Procedia Eng 2017;vol. 190:464–71. https://doi.org/10.1016/J.PROENG.2017.05.365.
[40] ANSYS, 'Mechanical APDL - Command Reference'. 2024.
[41] Zhang WF. Symmetric and antisymmetric lateral–torsional buckling of prestressed steel I-beams. Thin-Walled Struct 2018;vol. 122:463–79. https://doi.org/10.1016/J.TWS.2017.10.015.
[42] CEN, 'EN. -5, Eurocode 3 - Design of steel structures - Part 1.5: Plated structural elements'. European Committee for. Stand, Bruss, Belg 1993:2003.
[43] Sonck D, Boissonnade N, Van Impe R. Instabilities of cellular members loaded in bending or compression. Proc Annu Stab Conf - Struct Stab Res Counc 2012.
[44] Kwani S, Wijaya PK. Lateral torsional buckling of castellated beams analyzed using the collapse analysis. Procedia Eng 2017;vol. 171:813–20. https://doi.org/10.1016/J.PROENG.2017.01.370.
[45] ECCS, Ultimate limit state calculation of sway frames with rigid joints. Brussels, Belgium: European Convention for Constructional Steelwork, 1984.
[46] Teixeira FB, Caldas RB, Grilo LF. Influence of different shapes of geometric imperfections on the structural behavior of beams with large web openings. Adv Steel Constr 2020;vol. 16(3):272–8. https://doi.org/10.18057/IJASC.2020.16.3.8.
[47] Sonck D, Vanlaere W, Van Impe R. Influence of plasticity on lateral-torsional buckling behaviour of cellular beams. Mater Res Innov 2011;vol. 15(Suppl. 1). https://doi.org/10.1179/143307511×12858956847958.